GTRI Project A-5133

FINAL TECHNICAL REPORT
For Period 15 October 1995 - 31 March 2000

PROPOSAL FOR IN-SITU DETERMINATION OF ACOUSTIC PARAMETERS OF NAVY COATINGS FOR MOLD-IN-PLACE APPLICATION

Author
John Doane

Prepared for

Office of Naval Research
Program Officer Gary M. Jebsen ONR 334
Ballston Centre Tower One
800 North Quincy Street
Arlington, VA 22217-5660

Under
Grant No. N00014-96-1-0175

Prepared by

GEORGIA INSTITUTE OF TECHNOLOGY
A Unit of the University System of Georgia
Georgia Tech Research Institute
Atlanta, Georgia 30332

31 March 2000

Home of the 1996 Olympic Village
Georgia Tech Research Institute

List of Figures

I. Introduction

The United States Navy uses synthetic coatings for various purposes on a variety of ships. These coatings are typically viscoelastic polymers that are prepared and applied to the vessels in the shipyard during some phase of construction.

The coating begins with its constituent parts separated, some of which are solid and some liquid. The components are mixed and the product applied to the hull is a highly viscous liquid. A crawling apparatus moves from top to bottom depositing a strip of coating to the hull. The crawler then moves over and applies a strip adjacent to the previous one. The liquid cures very quickly into a solid form thus retaining the desired thickness on the hull. The proportions, mixing, and application of the constituents must be done with a high degree of accuracy and consistency in order for the final coating layer to meet performance expectations. Any errors in the mixing or delivery process will result in affected material properties such as Young's and shear modulus.

Currently, a coring method is used to determine the quality of the pour. In this method a sample of the coating is removed from the layer after the pour is complete and is then sent to a laboratory where various material property measurements are made on the sample. It is assumed that the properties of this core are representative of the layer as a whole. The area from where the sample was removed is then patched or filled with leftover material. There are several disadvantages to this

methodology: 1) it is destructive 2) it is a local or point measurement only 3) there is a delay caused by the need to send the sample to a laboratory. The first disadvantage, the destructive nature of the methodology, is undesirable because it creates a discontinuity in the surface and introduces additional interfaces in the coating layer. The second disadvantage, the local nature of the measurement, is undesirable because it returns the properties for a very small region of the coating. If the properties varied as the pour progressed, the properties far away from the core location might be significantly different. The third disadvantage, delay, is undesirable because it does not provide for quality assurance during the process. That is, if the process suddenly began to stray outside of desired parameters, the operators may not know until days after the pour is completed. Only later would the failure be known and a large balance of the pour would fail acceptance criteria.

This research proposes a different method for determining material properties that avoids the aforementioned disadvantages of the current system. The proposed system would avoid the destructive disadvantage by using a non-contact sensor for detection of signals generated by a surface contacting, but not penetrating, shaker. The proposed system would avoid the local disadvantage by making measurements that would test material properties over a significant spatial range and repeating these measurements at many locations over the entire surface. The proposed method would avoid the delay disadvantage by processing the data

quickly enough to alert the operators in time to halt and fix the process very shortly after the pouring system strayed.

The work presented in this report represents progress made up to the point of termination of the project due to funding considerations. Although only 43% of the contract value was funded, the major goal of identifying a method for determining material properties has accomplished and application of the technique developed here to several other related problems has been identified and one of those investigated. (see "VII. Comments and Conclusions" for a listing of these additional applications and "VI. Results" for a presentation of the data taken and modelling done in pursuit of one of these alternate applications). These alternate applications were discovered and the one pursued without a prepared out-of-specification sample which was one of the original contract items not delivered due to funding considerations.

II. Optimization Approach

The technique proposed here for the determination of material properties is the use of an optimization process. In this process measured data is quantitatively compared to the results from a theoretical model whose inputs include the properties of the subject material. An iterative process is used to intelligently vary the input parameters in order to improve the correlation of the theoretical model results to the measured data, thereby determining the material properties.

The object of comparison is a transient sinusoidal signal. Although the theoretical model is better suited to a continuous wave, a transient was necessary due to the finite dimensions of the test sample. The technique calls for a single cycle of the pulse to be delivered to the free surface of the sample and its propagation recorded by measuring the surface velocity at discrete (small) points along the surface of the sample radiating outwards from the epicenter. The measurement system records data in the time domain and then the data processing transforms the recorded data into the frequency domain.

The theoretical model takes the geometry of the sample, its constraints, the frequency of oscillation, position of interest, and the material composition as its input variables. The output is the surface velocity at the position of interest and the inputted frequency. This result is a continuous wave result, so a convolution with the input signal is necessary to predict the transient response.

At this point in the procedure there are experimental and theoretical data for each position and frequency in the range of interest which is determined by the power spectrum of the input signal. The experimental data are pairs of complex velocities, one being the component normal to the surface of the polymer layer and the other being parallel to the surface. An automated optimization routine then varies the material properties and searches for a smaller error between the experimental and theoretical results until a predetermined convergence value is achieved. A schematic of the optimization routine is shown in figure 1.

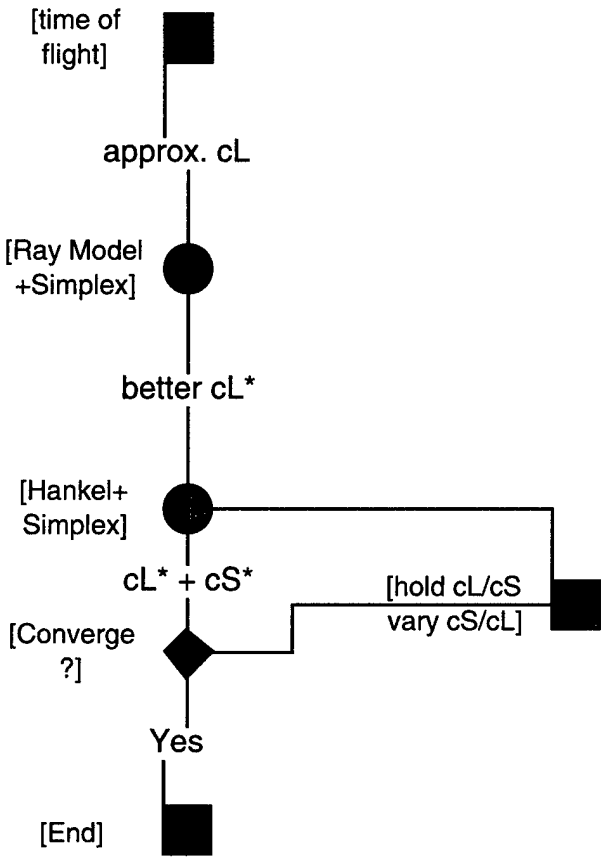

figure 1: optimization routine schematic

III. Experimental Setup

For this research the sponsor provided a test specimen of the subject polymer. It was a two inch thick slab with thirty inch sides. The slab was attached using epoxy to a two inch thick steel substrate plate with thirty-six inch sides.

(see figure 2)

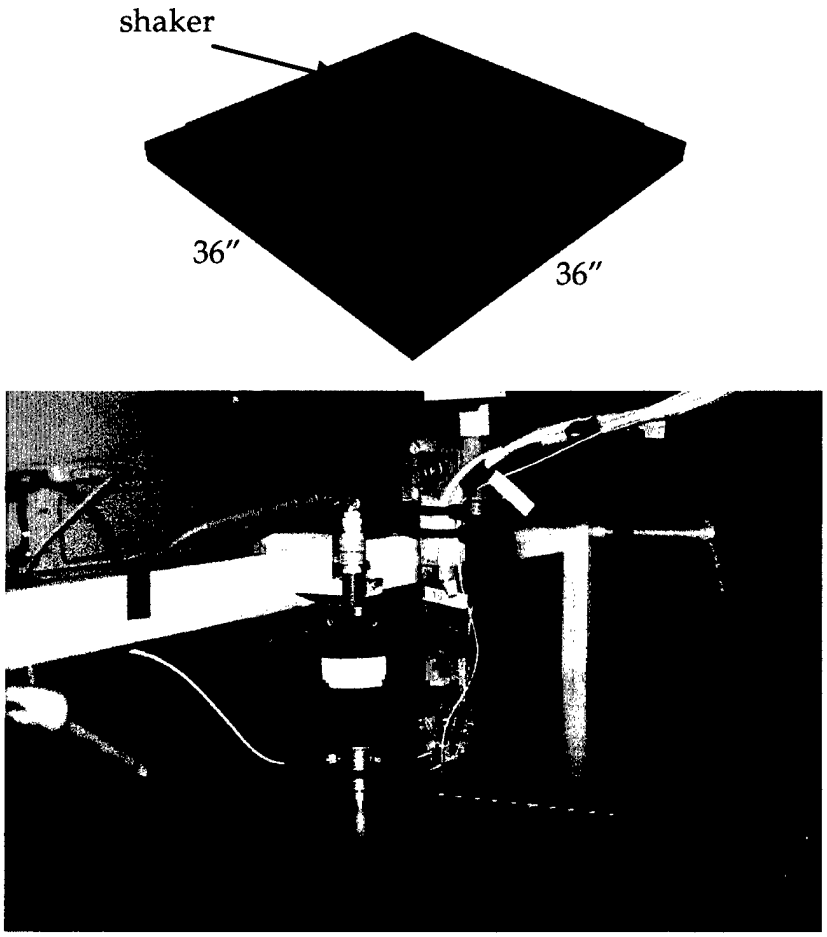

figure 2: sample mounted on steel backing plate with shaker and LDV probe positioned on the free surface of the test sample

The detection system was a Laser Doppler Velocimeter with a two-axis detection head capable of measuring the in-plane (parallel) velocity

and out-of-plane (normal) velocity in near simultaneous fashion. (see Appendix A for details of the LDV system). The head used fiber optic connections and was mounted on a computer-controlled positioning device that allowed for precise spacing between the measurement points and convenient focusing. Time domain waveforms were digitized using a Tektronix 2430A oscilloscope and a GPIB connection used to transfer the data to a computer for storage and analysis.

A Bruel & Kjaer model 4810 mini excitation shaker was used to generate the waves input to the sample. A Wavetek 275 Signal generator created the electrical signal that drove the shaker using one cycle of a sine wave at 2 Kilohertz. An accelerometer was mounted to the head of the shaker and served as the contact surface for imparting the disturbance into the slab. See figure 3. The accelerometer signal was recorded and digitized for use during processing.

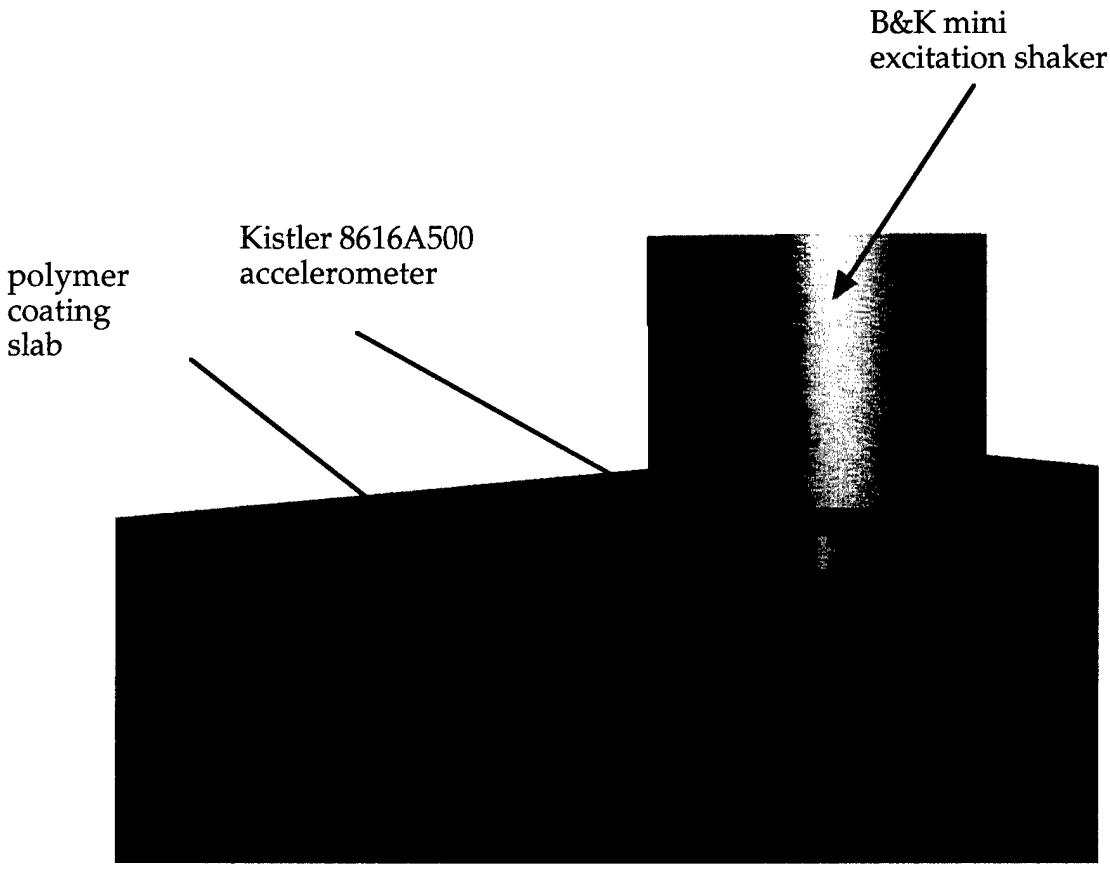

figure 3: illustration of the B&K shaker resting on the coating slab surface

The shaker was placed approximately in the middle of the slab and measurement locations identified radially extending from the epicenter, as shown in figure 4. Measurement point 1 is 0.064 meters from the epicenter and subsequent locations are spaced at 0.5" (0.0127 m) intervals. Accurate spacing was achieved by using the stepper motor controls attached to the positioning arm to which the probe head was attached.

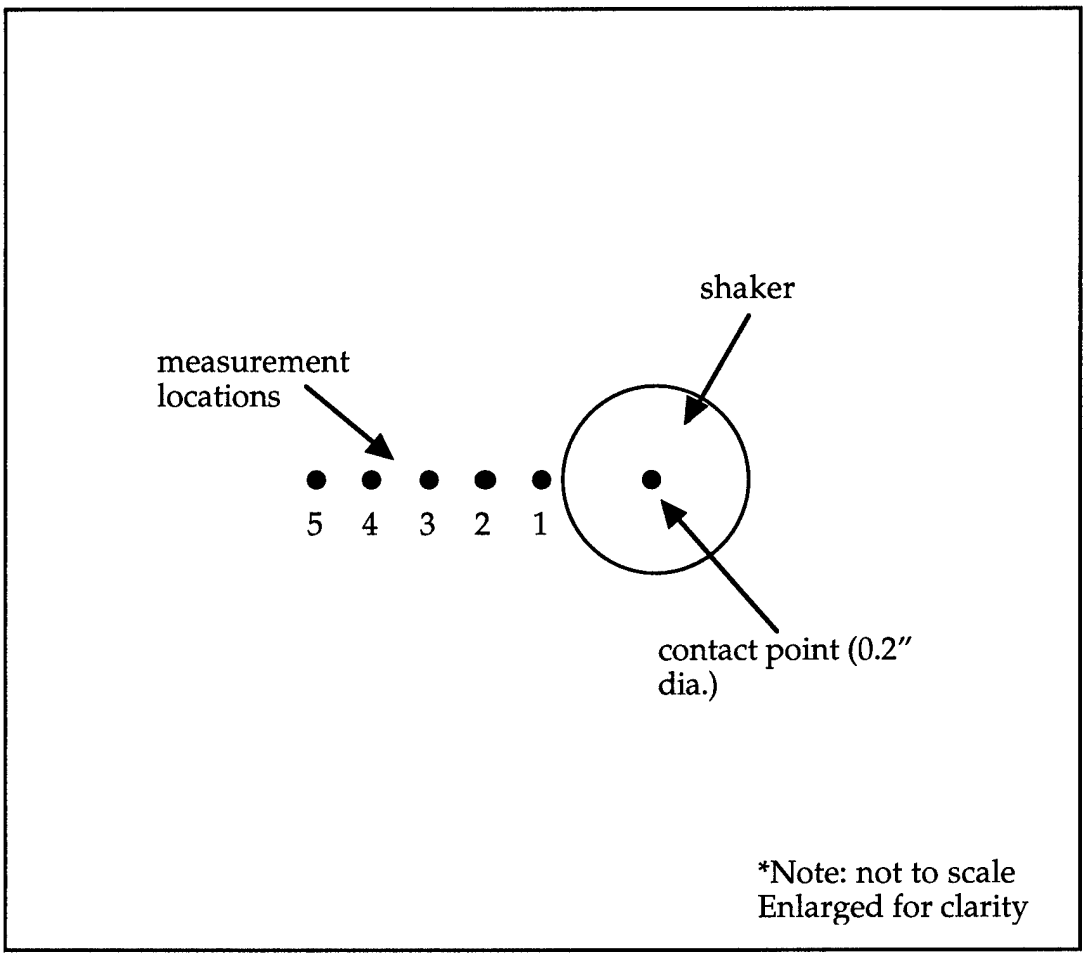

figure 4: LDV measurement locations

IV. Theoretical Modelling

Several theoretical models were investigated and used in varying degrees for this research. A simple ray acoustics model was used for basic investigation and seed values for the more complex model (see **V. Optimization Process**). A model by Miller and Pursey[1] was used for initial comparisons and understanding of the basic wave structure. The limitation of this model is that it considers only the case of a free half-space. For the final processing a model developed by Weaver[2] was used since it was completely applicable in terms of geometry and input variables.

The geometric ray acoustics model used a theoretical input signal that closely approximated the actual input. One cycle of a two kilohertz sine wave was generated in the Matlab® computational environment. To improve its relation to the actual signal a Hanning window was applied, effectively removing the first-derivative discontinuity at the beginning and end of the cycle. This discontinuity does not exist in the physical signal since the acceleration of the shaker head is not instantaneous. This waveform was then replicated three times, each using a different delay and decay based on the appropriate wave speed and attenuation value (in addition to spherical spreading). The three formed cycles correspond to the direct arrival of the compressional wave, the direct arrival of the shear wave, and the arrival of the compressional wave after reflection off of the

[1] G.F. Miller and H. Pursey, "The field and radiation impedance of mechanical radiators on the free surface of a semi-infinite isotropic solid". The National Physical Laboratory, Teddington, Middlesex.
[2] "Transient ultrasonic waves in a viscoelastic plate: Theory". Richard Weaver, Wolfgang Sachse, and Lin Niu, Department of Theoretical and Applied Mechanics, Cornell University, Ithaca, New York

coating-steel interface. The polarity of the formed signals was matched to the directionality of the LDV probe. (see Appendix A for details of the LDV system). The formed cycles were then combined to create a composite signal.

The Miller and Pursey model is an adaptation of Lamb's method designed to furnish definite integral representations of the field at an arbitrary point in a semi-infinite isotropic solid due to prescribed periodic stresses on the free surface. The equation of wave propagation in an isotropic solid is given here:

$$c_{11}\nabla\nabla.\bar{u} - c_{44}\nabla x \nabla x\, \bar{u} = \rho\frac{\partial^2 \bar{u}}{\partial t^2}$$

equation 1: wave propagation in isotropic solid

where

u - displacement

c11 - compressional elastic constant

c44 - shear elastic constant

ρ - density of the medium

Solution of this equation solved for the boundary condition of a circular disk vibrating normally to the free surface yields the following equations.

$$u_z = \frac{a}{c_{44}} \int_0^\infty \frac{\sqrt{(\zeta^2 - 1)} J_1(\zeta a)}{F_0(\zeta)} \left\{ 2\zeta^2 e^{-z\sqrt{(\zeta^2 - \mu^2)}} + (\mu^2 - 2\zeta^2) e^{-z\sqrt{(\zeta^2 - 1)}} \right\} J_0(\zeta r) d\zeta$$

equation 2: Miller and Pursey result for circular disk vibrating normally to the free surface (out of plane displacement)

where

a - radius of driving piston

ζ - integration variable

$$\mu = \sqrt{\frac{c_{11}}{c_{44}}} = \frac{k_2}{k_1} = \sqrt{\frac{2(1-\sigma)}{1-2\sigma}}$$

where

σ = Poisson's ratio for the medium

and $F_0 = (2\zeta^2 - \mu^2)^2 - 4\zeta^2 \sqrt{(\zeta^2 - 1)} \sqrt{(\zeta^2 - \mu^2)}$

The equation for the radial displacement is similar. Note that the input variables are the complex moduli, driving piston radius, and the radial and axial position of the evaluation point. An example of the results from this model is shown in figure 5.

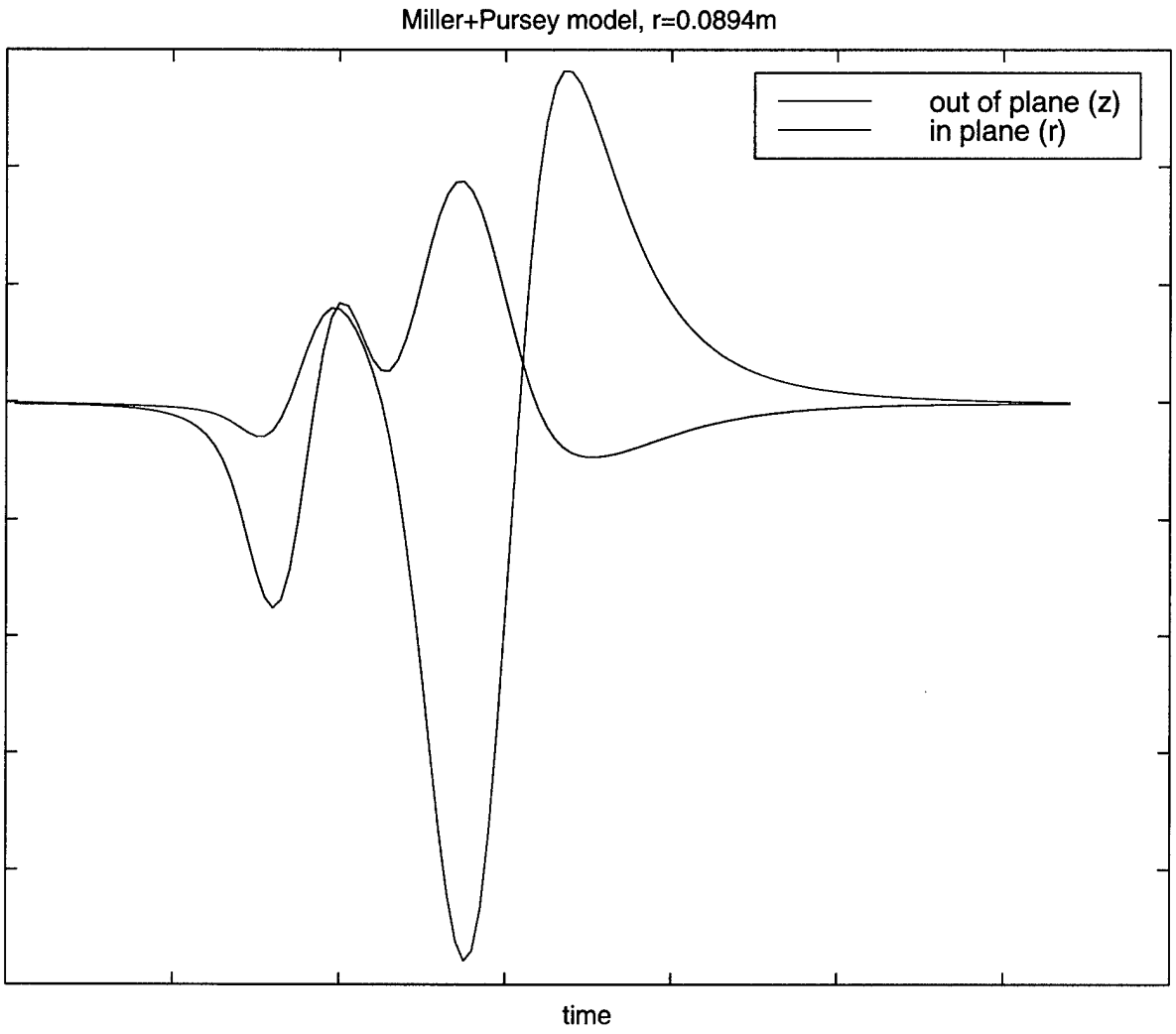

figure 5: result of the Miller and Pursey model
for r=0.0894 m, in plane and out of plane displacement

This model was used to gain an understanding of how the changes in modulus value affected the shape of the output signal. This was useful in examining the structure of the measured waveforms in order to develop analysis procedures, particularly the use of the ray model in determining approximate seed values for the Simplex optimization procedure. (see **V. Optimization Process**).

The third model used was the one developed by Weaver, Sachse, and Niu with the stated goal of determining the nearfield response of a thick viscoelastic plate at epicenter, off-epicenter, and on the same side of the plate to a point step load acting normal to the surface.[3] In their derivation, the test "object" is a homogeneous infinite flat slab of thickness 2h (=H) with free surfaces at z=±h subjected to a concentrated downward force:

$$\tau_{zz} = -\frac{1}{2\pi r} F\theta(t)\delta(r)$$

where

$\theta(t)$ = step function in time

$\delta(r)$ = delta function in space

equation 3: force applied to free surface in the Weaver model

The displacement potentials ϕ and ψ are defined by

$$u = \frac{\partial \phi}{\partial r} - \frac{\partial \psi}{\partial z}$$

$$w = \frac{\partial \phi}{\partial z} + \frac{1}{r}\frac{\partial (r\psi)}{\partial r}$$

equation 4: displacement potentials for Weaver model

where

u = radial displacement field

[3] "Transient ultrasonic waves in a viscoelastic plate: Theory". Richard Weaver, Wolfgang Sachse, and Lin Niu, Department of Theoretical and Applied Mechanics, Cornell University, Ithaca, New York

w = vertical displacement field

The solution for the vertical displacement field is given in the frequency domain in terms of the Fourier transformed normal displacement.

$$\hat{w}\big|_{(z=\pm h,r,\omega)} = -Q\frac{\omega^2}{c_s^2}\int_0^\infty k\alpha J_0(kr)\left(\mp\frac{\sin(\beta h)\sin(\alpha h)}{R_s}+\frac{\cos(\beta h)\cos(\alpha h)}{R_a}\right)dk$$

equation 5: result of inverse Hankel transform for the vertical displacement field

This equation is then integrated over all values of k to achieve the final answer. There is some difficulty, however, in that the high wavenumber portion of the integral does not necessarily converge absolutely. To overcome this convergence problem an analytical expression is used to cover this region of the integration.

$$\int_L^\infty J_0(kr)dk \approx \frac{\sqrt{(2/\pi)}}{r\sqrt{Lr}}\left[-\sin\left(Lr-\frac{\pi}{4}\right)+\frac{5}{8}\left(\frac{1}{Lr}\right)\cos\left(Lr-\frac{\pi}{4}\right)+\ldots\right]$$

equation 6: analytical expression for high wavenumber portion of the integrand in Weaver's model

To evaluate this solution, the appropriate input was needed in addition to material properties and geometries. Additionally, a boundary condition had to be changed from the free-free condition previously existing to a rigid boundary condition assumed on the lower surface

where the slab was attached to the steel plate.

The theoretical input used a step function in time which was inappropriate for the experimental conditions which used a one cycle sine wave. To utilize a more accurate input force for the equations, the recorded and digitized input signal was used in place of the step function. Additionally the boundary condition at the lower surface of the slab was not appropriate for the experiment that was conducted. The theory treats the lower surface as free whereas the experimental conditions have it as (nearly) rigid. When this change of boundary conditions is addressed and the theory reformulated, the integrals to be determined are as follows.

$$\hat{u}_r(r,\omega) = \int_0^\infty \frac{(\beta d_1 - d_2) J_1(a\xi)}{(2\xi^2 - k_2^2) d_2 - 2\xi^2 \beta d_1} J_1(r\xi)\xi d\xi$$

where

$$d_1 = -\alpha + \frac{2\alpha}{2\xi^2 - k_2^2}\xi^2 \cos(\alpha' L)\cos(\beta' L) + \frac{2\alpha}{2\xi^2 - k_2^2}\alpha\beta \sin(\alpha' L)\sin(\beta' L)$$

$$d_2 = \frac{2\alpha}{2\xi^2 - k_2^2}\beta\xi^2 - \left[\alpha\beta\cos(\beta' L)\cos(\alpha' L) + \xi^2 \sin(\beta' L)\sin(\alpha' L)\right]$$

$$\alpha = \sqrt{\xi^2 - k_1^2} = i\alpha'$$

$$\beta = \sqrt{\xi^2 - k_2^2} = i\beta'$$

ξ is the Hankel transform variable

a is the drive piston radius

Similarly, the vertical displacement integral is given next.

$$\hat{u}_z(r,\omega)=\int_0^{\infty}\frac{\xi^2\dfrac{2\alpha}{2\xi^2-k_2^2}-\alpha}{\left(2\xi^2-k_2^2\right)-2\beta\xi^2\dfrac{2\alpha}{2\xi^2-k_2^2}}\frac{J_1(a\xi)}{\xi}J_1(r\xi)\xi d\xi$$

equations 7: final Weaver integrals

The integrals were then evaluated over a range of frequencies for which the measured input signal had energy (spectral range). These result were then inversely transformed into the time domain for qualitative comparison.

A sample time domain result is shown in figure 6.

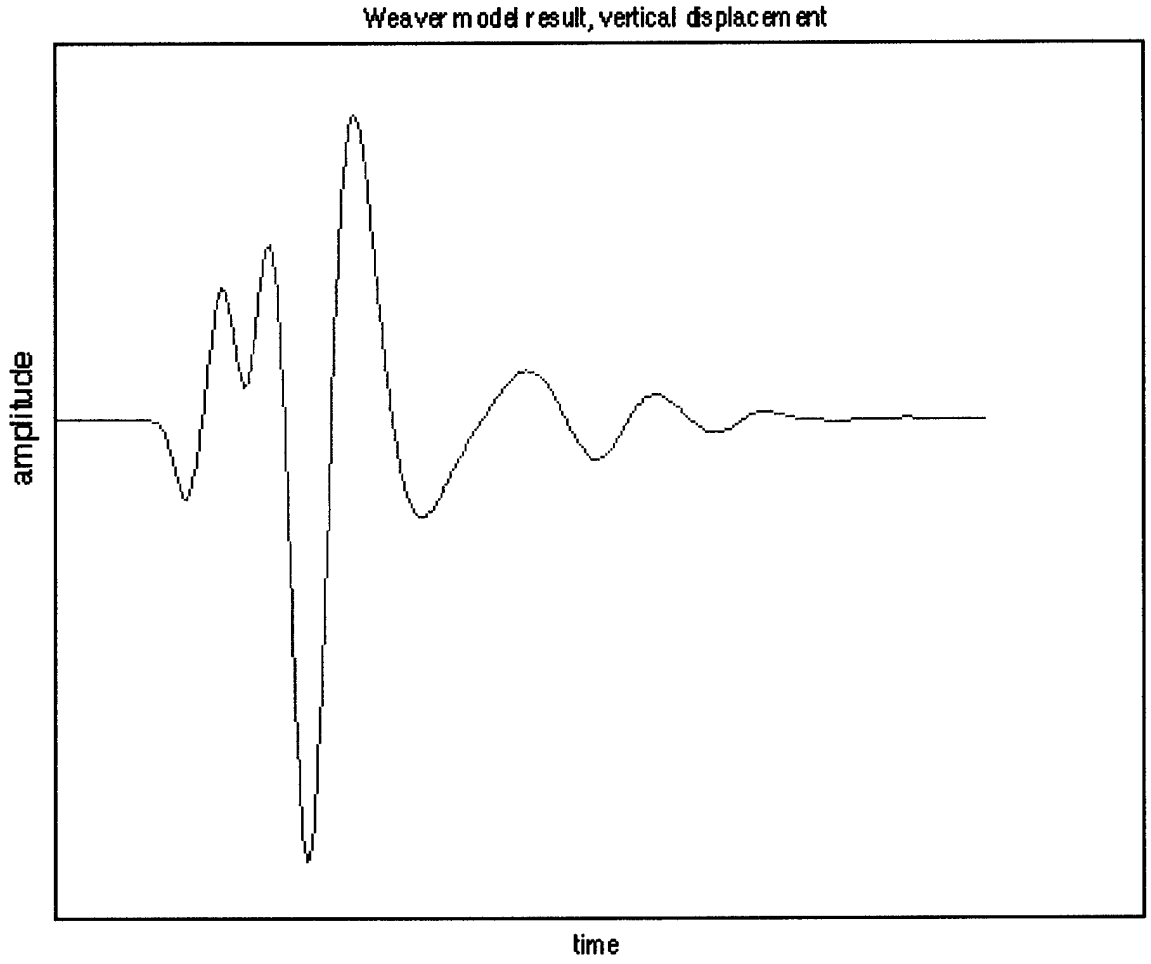

figure 6: Weaver model result for vertical displacement

V. Optimization Process

In order to systematically vary the input parameters to improve correlation between measured and calculated results a Simplex routine was implemented. This algorithm operates by changing the size and shape of an object in an n-dimensional solution space where n-1 equals the number of variables being solved for. The process requires an initial n-number of solution sets as a starting point but the resulting shape need not bound the actual solution thereby making it a very robust optimization process. The routine then computes a single performance metric for the current solution sets. If the metric does not meet a prescribed success tolerance, it automatically reshapes the solution volume by moving the vertex which had the poorest performance in the previous iteration. Eventually, as the solution volume converges around the solution, the solution volume shrinks and the vertices converge to the final value. For more information on this technique, refer to Numerical Recipes: The Art of Scientific Computing. (New York: Cambridge University Press, 1986). Appendix C of this document lists the code used and a sample Simplex solution.

This technique was chosen for its robust nature and its ease of programming. Test cases were performed on two-dimensional problems so that the progress of the algorithm could be monitored by plotting the solution volume, in this case a triangle, on an x-y plot. It was then easy to build confidence in the routine as its convergence was monitored for this test case. A disadvantage of the routine is that it requires an initial solution

volume near but not necessarily encompassing the actual solution in order to avoid becoming trapped in a local minima.

To initiate the Simplex routine for the case at hand a procedure was needed to determine approximate material parameters that does not require an initial guess. To do this, a simple geometric acoustics ray model was employed in conjunction with time of flight measurements.

The Ray model is a simplification that does not include all of the physics involved in the situation. However, it is sufficient as a means of calculating initial guess values for the Simplex procedure operating on the Weaver model. The Weaver model (in conjunction with a variation on it for a half-space by Miller and Pursey) showed that the fastest wave traveling along the free surface of the slab is directly related to the plane wave modulus. Given this, it is reasonable to use the first half-cycle of the recorded signal to determine the longitudinal speed of the material. By measuring the result at five locations extending along a radial away from the epicenter it is possible to also get an estimate of the attenuation. To do this, the ratio of the amplitudes of the successively recorded waves were calculated and the decrease due to spherical spreading removed. The remaining decrease was attributed to viscoelastic loss in the material. By doing this calculation in the frequency domain on a per-frequency basis the effects of dispersion are automatically accounted for since the results, both speed and attenuation, are at discrete frequency points.

The wave constituents considered in the geometric ray model were

the direct longitudinal wave, the direct shear wave, and the reflection of the longitudinal wave off of the interface with the steel plate at the bottom of the slab. A sample result is shown in figure 7.

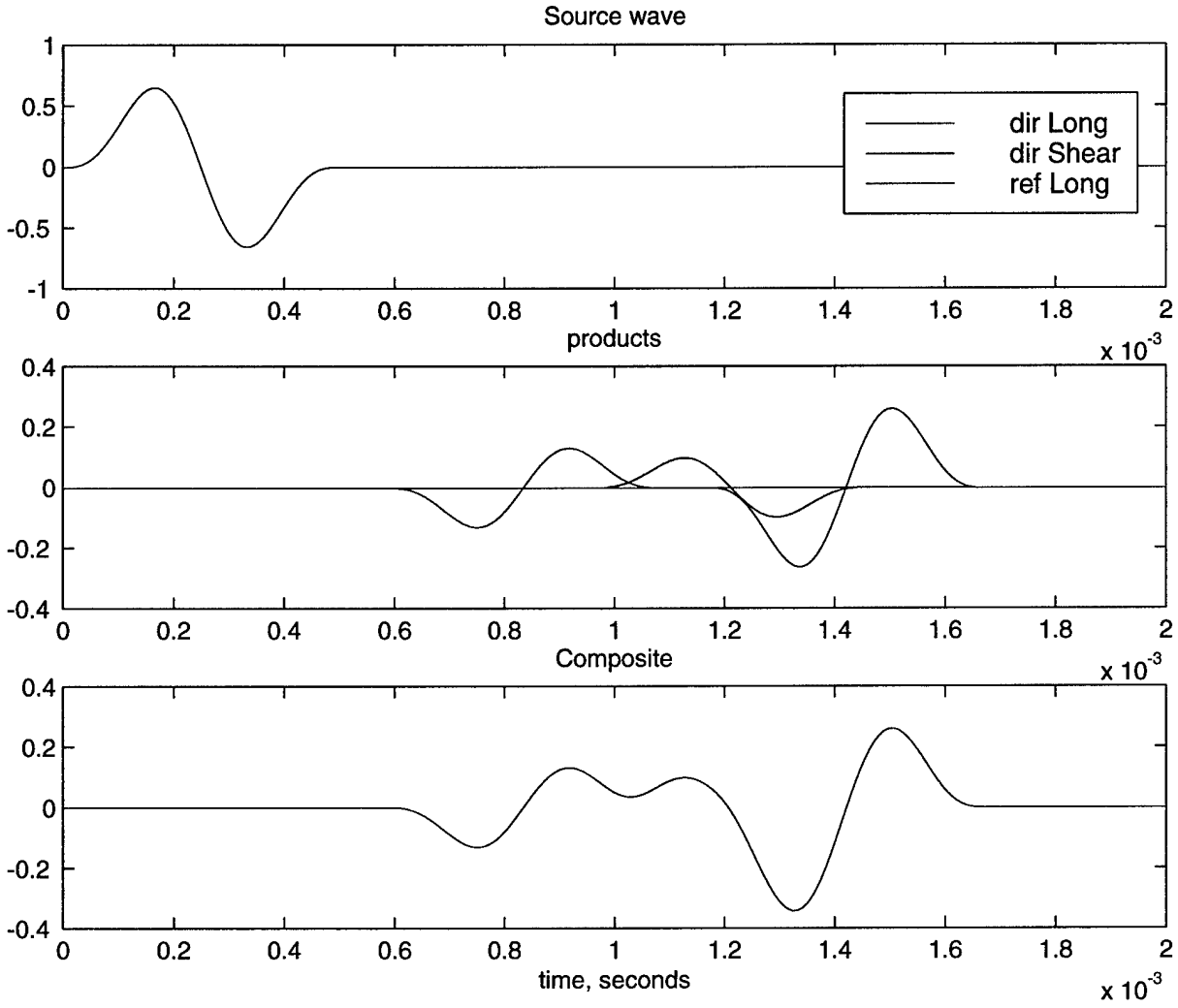

figure 7: Ray model result

For comparison, the ray model was run and its results compared to the LDV data taken for the third measurement point, shown in figure 8.

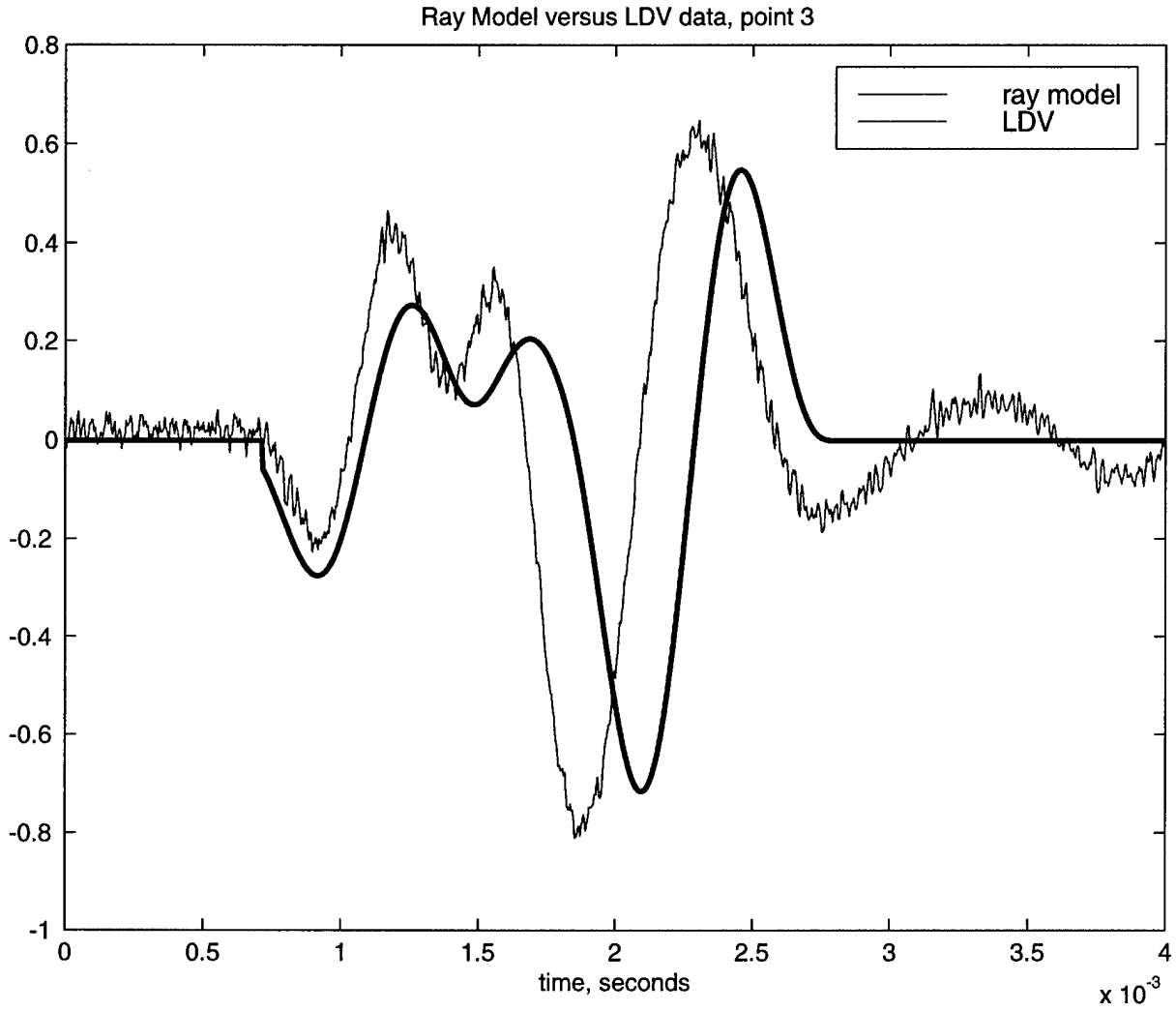

figure 8: ray model result overlaid with LDV for point 3

VI. Results

The shaker used to excite the coating slab had an accelerometer mounted to its head and was therefore in direct contact with the coating during the excitation. The recorded signal from the accelerometer was used in the theoretical calculations and is shown in figure 9.

The LDV system was used to record waveforms at the measurement points for both in-plane and out-of-plane motion. Those recorded signals are shown in figures 10 and 11.

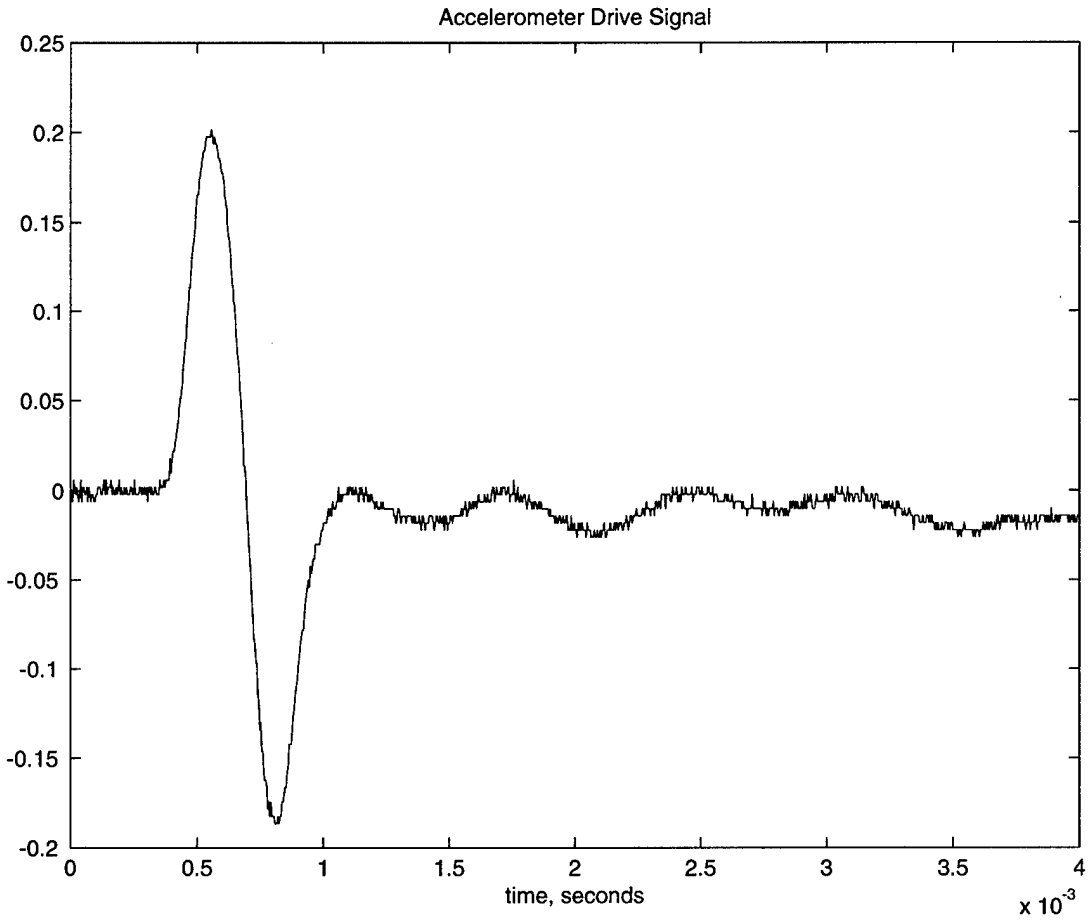

figure 9: accelerometer signal

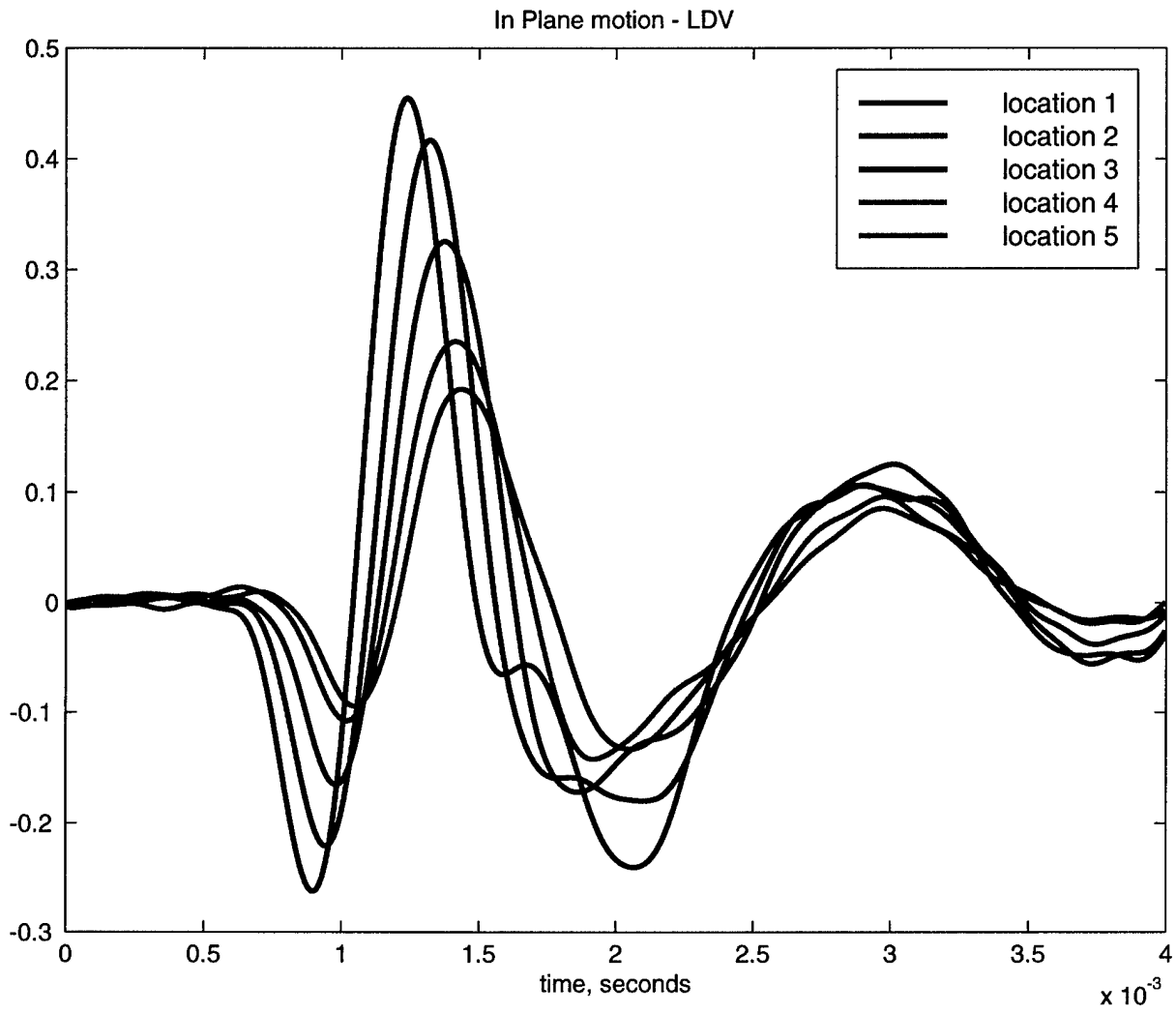

figure 10: In Plane motion signals detected by LDV

In figure 10 there are five plots shown for data taken in the time domain. The first location is at a position located 0.064 meters from the epicenter. (refer to figure 4, page 13). Each subsequent point (2-5) is taken at a location 0.0127 m further away from the epicenter on a line extending radially away from the epicenter.

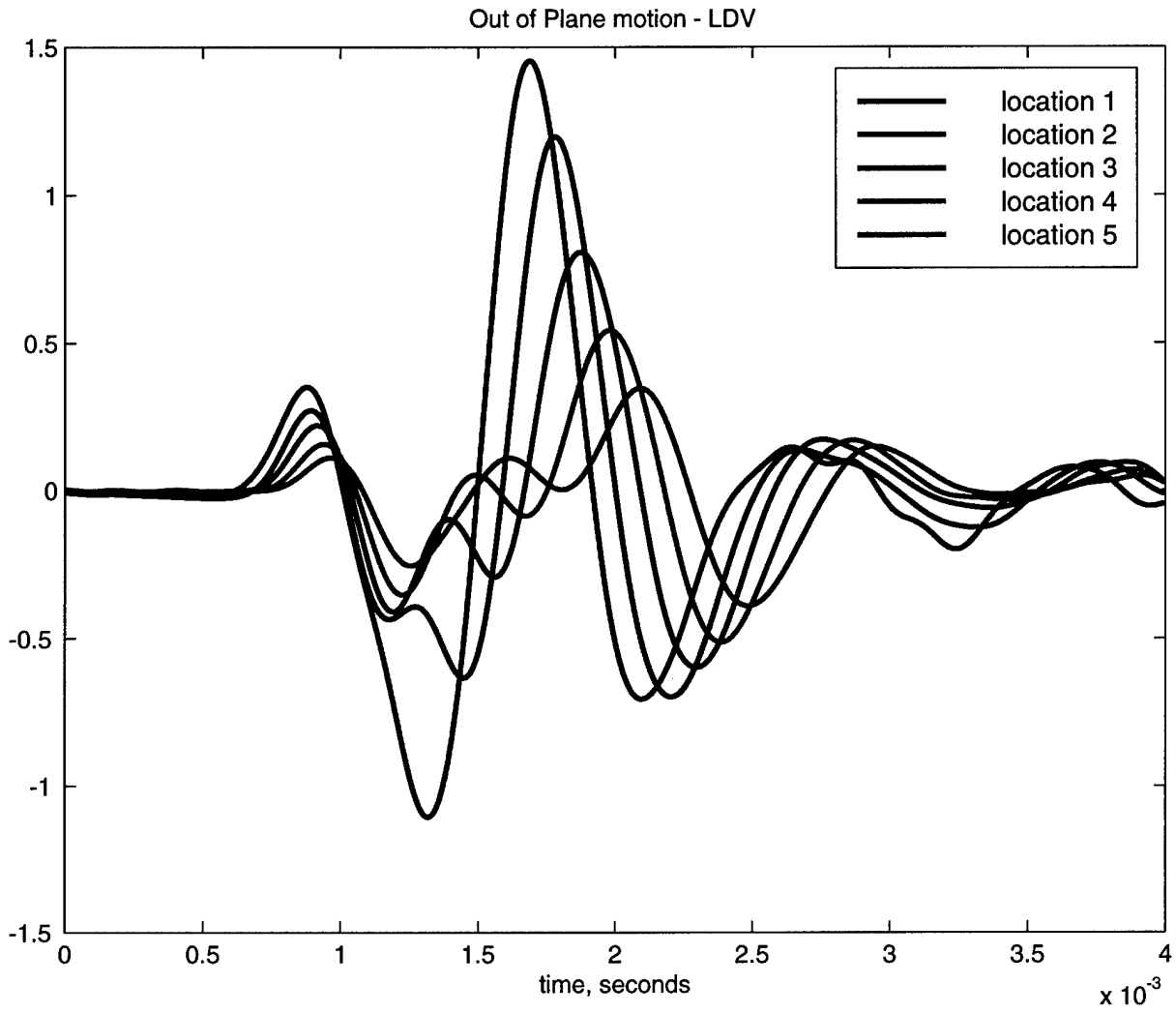

figure 11: out-of-plane motion signals detected by LDV

Weaver model in-plane and out-of-plane results for all five location points are presented in figure 12.

The results of the Simplex convergence are shown in figure 13 and 14.

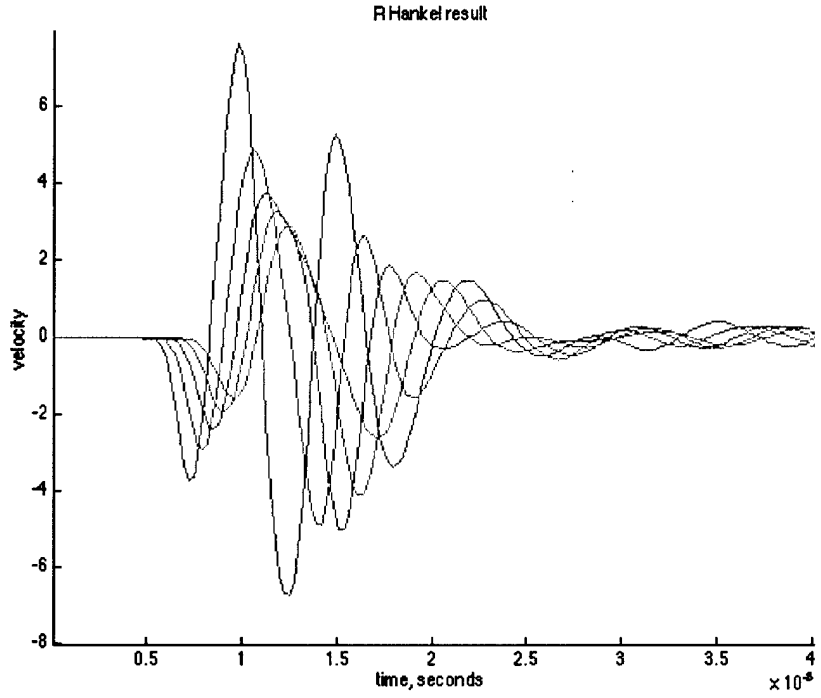

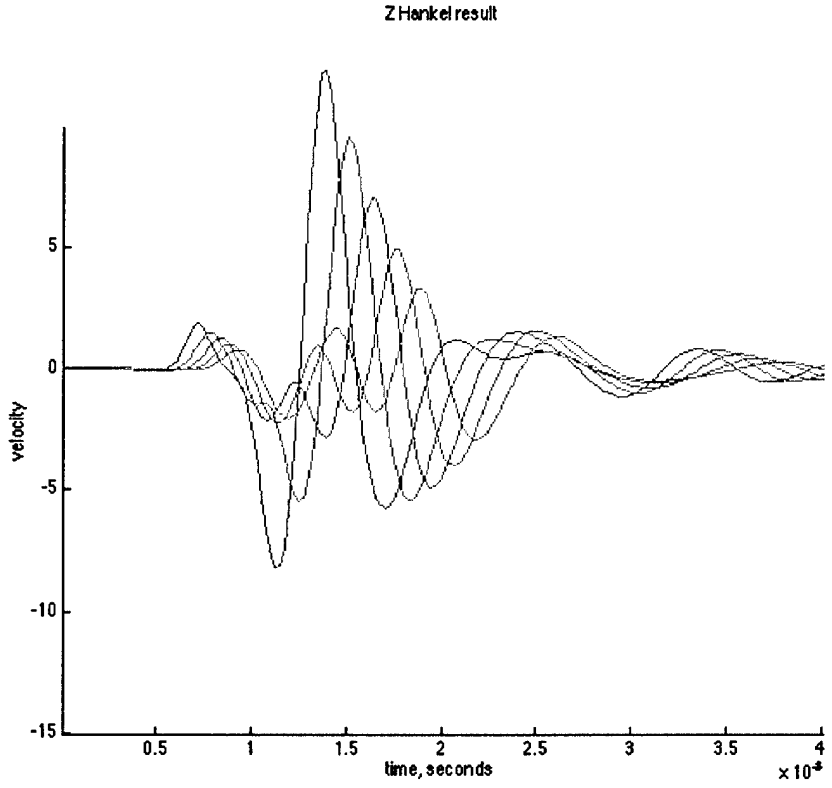

figure 12: Weaver results for R (in-plane) and Z (out of plane)

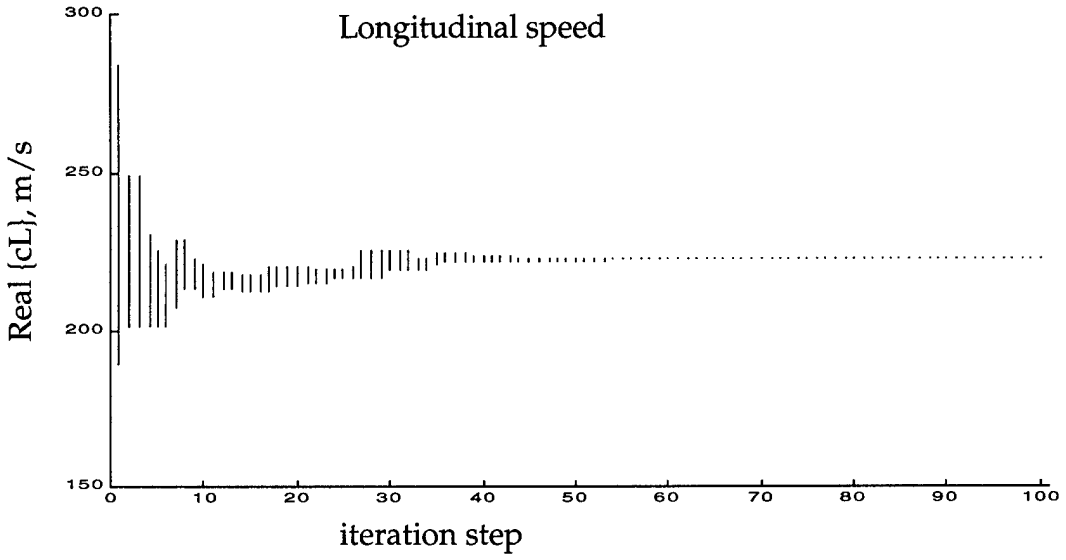

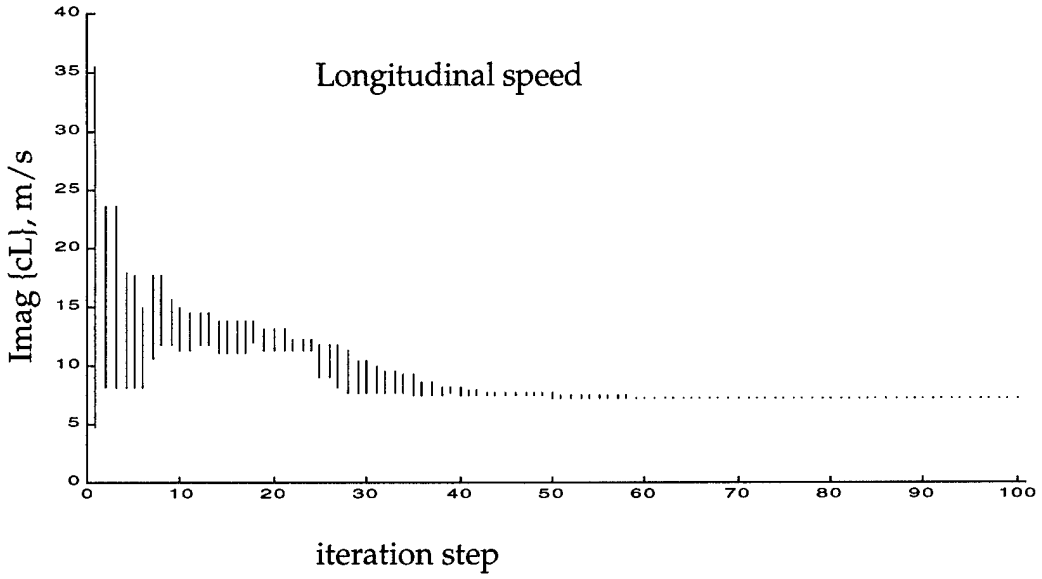

figure 13: Simplex convergence for Longitudinal speed

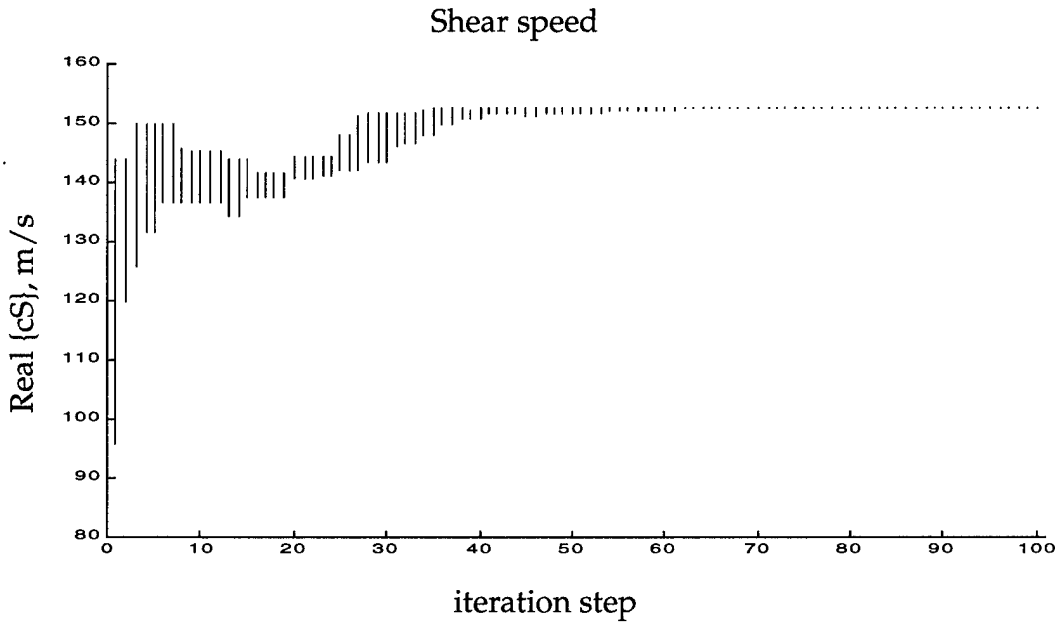

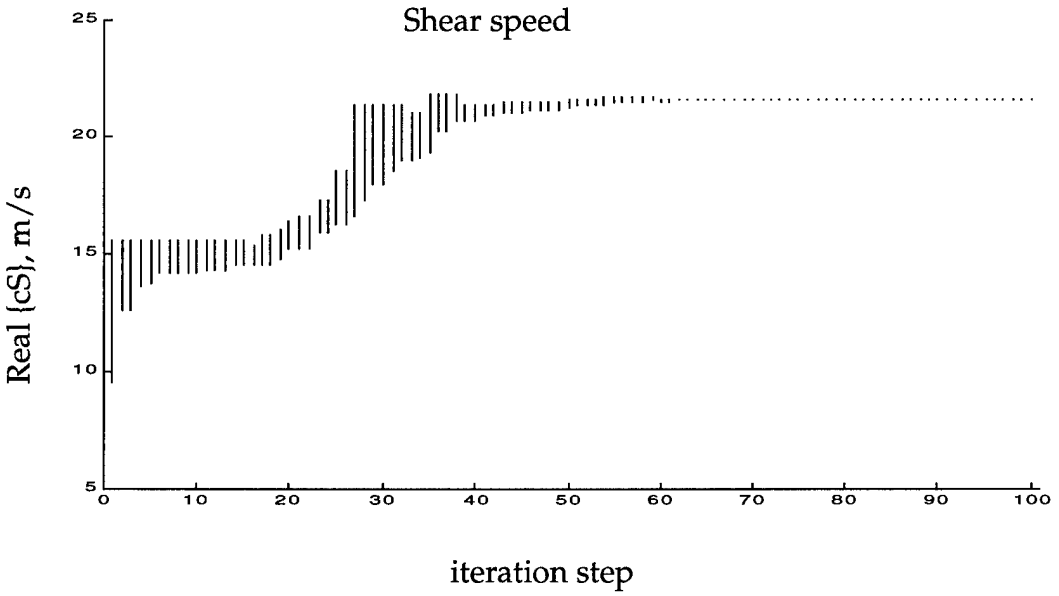

figure 14: Simplex convergence for Shear speed

For comparison, shear modulus data was obtained from an experiment using a different method of measuring material properties on

the same subject material.[4] A comparison table is presented below.

	Hankel Model + Simplex	Conventional Method
frequency, Hz	977	1100
Shear speed, m/s	153 +i 21.7	126 +i 29.4

table showing a comparison of the results for the shear speed from a conventional method to the one presented here

Please see "Comments and Conclusions", section VII, for a discussion of these results and their comparison.

Although the original goal of the program was to develop a technique for measuring material properties, a tangential application of the experimental technique developed here was briefly explored.There is great interest in the detection of voids or occlusions in a poured layer which can come from either air bubbles or coagulated deposits of a constituent material. In either case the acoustical transmission through the coating layer is adversely affected by the presence of occlusions. Due to the difference in density and elastic properties, sound waves will scatter off of occlusions and thus provides a means of detection. The LDV system was used to measure wave propagation in a pair of samples made from the same material used in the body of this research. A 0.5" wide strip of the

[4] Willis, Richard Lance. "Non-Invasive Characterization of Micro-voided Polymers Under Controlled Static Pressure and Temperature Using Laser Doppler Vibrometry". Presented as a PhD thesis at the Georgia Institute of Technology, School of Mechanical Engineering, December 1999.

material was cut off of the main slab and mounted on a steel block with the same thickness as the mount plate for the slab. A hole was then drilled through the strip to simulate an occlusion being present in the material. The wave propagation through the region containing the occlusion was compared to propagation through unaltered material. The results show a noticeable difference and therefore an ability to detect their presence. See figures 15-17.

Although this application was not explored further it does show the versatility and potential usefulness of the technique. In addition to the occlusion detection, ideas for additional applications include bonding integrity and seam integrity analysis.

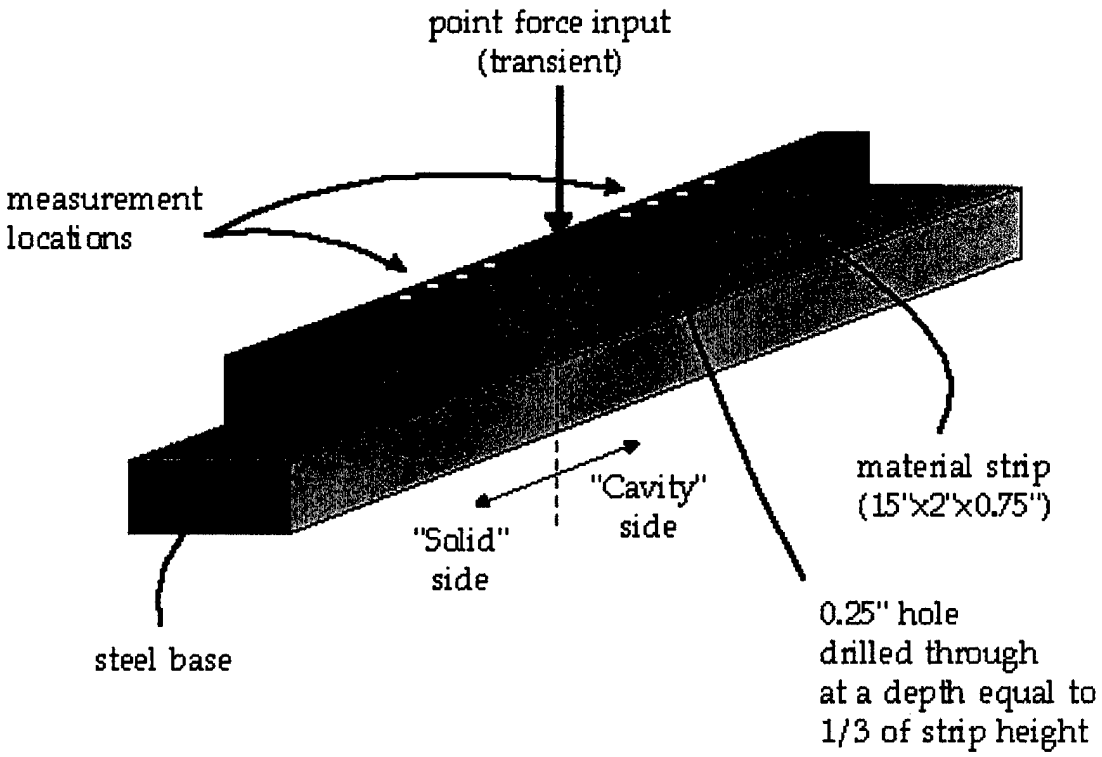

figure 15: occlusion detection test sample

Measurement Locations

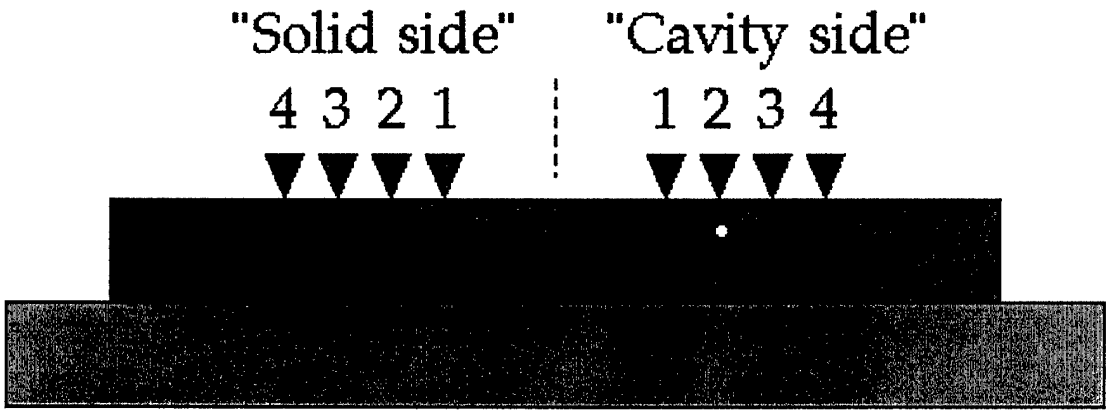

"Deep" cavity

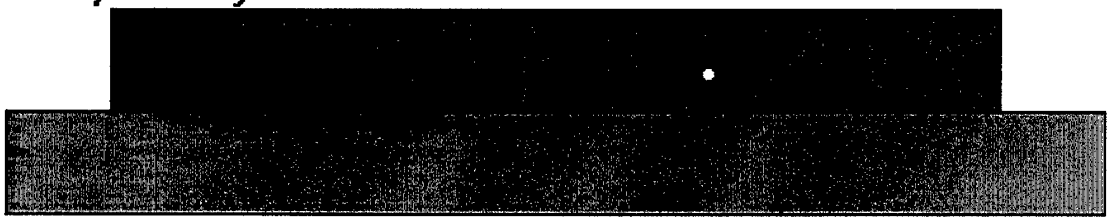

"Shallow" cavity

figure 16: nomenclature for occlusion detection

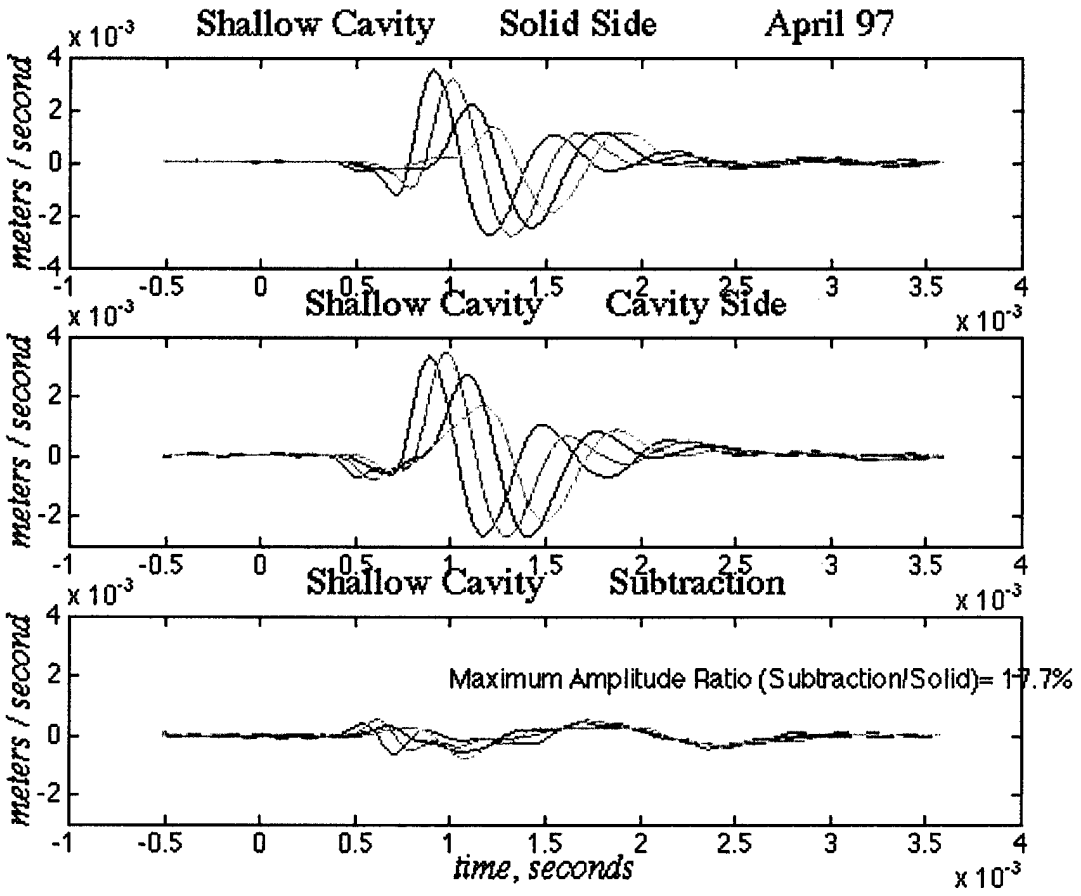

figure 17: results for shallow cavity detection

Although no analysis will be presented here, the presence of the occlusion can be detected qualitatively by observing the changes in the front end of the recorded waveforms from the "Solid Side" to the "Cavity Side". This difference is also plotted in the third plot, "Subtraction".

VII. Comments and Conclusions

The data presented in the results section reflects the best results obtained at the time of the suspension of research. Due to the nature of the experimental work it was not possible to test a known material and thereby confirm the accuracy of the technique presented. Likewise, the usefulness of the comparison to the conventional method is somewhat limited in that it was not tested against a known material either.

This technique was designed to be used in a demanding situation (bonded on one surface) and the success achieved is encouraging. There are three main items which should be addressed if better accuracy is desired from this technique in the future.

First, measurements should be made using a force gauge in the delivery chain. The Weaver model uses a stress input and the results obtained in this work used the acceleration signal for input. Although closely related, the differences in these measured quantities do create error.

Second, a better understanding of the Simplex method should be acquired. For complicated solution spaces like the one present in the integral solutions here, the initial input formulation is important so as to avoid false minima. Some investigation should be made into the merits of either a successive two-parameter search or a singular four-paramter search. Again, these two methods may have different behaviors in searching the complicated solution space.

Third, some investigation into the subtleties of the numerical integration should be made. The integrands in the present work exist in the complex plane with complicated behaviors. The numerical integration interval must be properly chosen and it is possible that a non-regular stepping would be advisable in order to properly resolve areas in which integrand values change rapidly. Additionally, the transition from the standard integral to the asymptotic form must be done at an optimum point. Further investigation of these issues may result in better output from the theoretical model.

Despite these areas of possible weakness, the combination of experimental and theoretical work presented here is considered successful. The Laser Doppler Vibrometry system worked well in obtaining the desired data for the technique. The theoretical models produced results that are expected and logically consistent. The output from the models compares well to the experimental data on a qualitative level, particularly shape and features of the waveforms. The quantitative results compared reasonably well with the other method and fit into the library of results for this type of material quite well.

Experience in fine-tuning design and operation of Laser Doppler Vibrometer systems was gained. As the system used for this work has also been used for previous and subsequent experimental work, the hardware constantly undergoes improvements. This research effort raised the level of sophistication and furthered knowledge of LDV hardware

design and usage.

Development of the theoretical models required learning a considerable amount about wave propagation in solids and numerical integration. The insight gained in this education has been valuable and will be applicable in any further work done in vibration and acoustics.

In addition to the alternate application of this technique presented in the Results section, there is potential application possibilities in the related problems of debonding and seam integrity.

Debonding occurs when the coating layer does not properly adhere to the steel plate substrate layer. This can be a disastrous circumstance since the portion of the polymer layer that is not secure to the hull may separate in the presence of viscous flow (as the boat moves through the water) and collide with apparatus aft of the area from which the coating section departed. This is another situation which would not become apparent until well after the coating application has been completed. The technique presented here would be able to investigate the bond integrity since part of the composite signal is due to the reflection off of the interface between the polymer layer and the steel plate. The reflection coefficient, which described the percentage of the energy returned into the coating after reflection, is dependent on the type of bond at the interface and is opposite in sign for the case of a completely debonded interface. There is also additional avenues of pursuit available for exploring this problem with the use of rotational shear (torsional) waves. Since the

particle motion in this type of wave is parallel to the interface plane there would be considerable impact on the reflection coefficient if the bond was poor or non-existent.

Seam integrity is a description of the adherence of adjacent coating strips to each other. (see introduction for a brief description of the application process). Poor seam integrity is problematic when the boat is underway since it may lead to failures that cause section of the coating to depart from the hull by allowing flow forces from the medium to peel the edge of a coating section up and eventually force an entire section to tear away from the hull. The technique presented here is applicable to investigating this failure mode since part or all of the composite signal received at the surface of the coating would travel across a seam if the transmit and receive elements were positioned on opposite sides of a seam. Poor seam adherence would manifest itself primarily by reduction in signal amplitudes due to the reflection of energy at the interface between poorly adhered adjacent coating strips. There may also be some distortion in the case of a marginal bond that would introduce new propagation dynamics into the signals.

These alternate applications of the technique may be a valuable use of the technology developed here since they might provide a binary ("yes" or "no") method for evaluating a given instance of coating application.

An additional consideration for the application of this research to

usable industry-grade technology is the work environment. The experiments involved in this research effort were conducted in a laboratory and as such were afforded favorable conditions that might not exist in an actual environment, e.g. a naval construction shipyard. Particularly, dust, noise, and vibration are variables that would affect the operability of such a system. To overcome these problems would involve significant refinement of the technology involved to improve its robustness not only in terms of physical strength but operational simplicity. The current state of the technology requires a knowledgeable operator conducting the experiment with vigilance which would not likely be available in the shipyard environment. However, it might be feasible to achieve this type of robustness for a binary-decision type of system described above.

Appendix A

LDV System Details

This research effort used a Laser Doppler Velocimeter already resident at Georgia Tech. It used a 35mW Helium-Neon laser as its light source and optical fibers to deliver the light to the test surface.

The basic operational principle of the Laser Doppler Velocimeter is to detect the change in frequency of the light reflected from a vibrating surface. The amplitude and phase of the surface velocity is determined from the measured Doppler frequency shift. These measured quantities can then be processed to determine the particle motion of the surface which is being illuminated by the focused laser spot.[5]

The general layout of the hardware is shown in figure 15. In the figure the components are labeled by letters from A-N. A description of each piece and its function is given here.

A: Helium-Neon laser; generates a coherent beam with a wavelength of 632.8 nanometers

B: Beamsplitter cube; reflects approximately 4% of the light to form a reference beam

C: Acousto-Optic modulator; a quartz crystal driven a 40MHz oscillator that is adjusted to split the light into many beams, two of which are approximately equal in amplitude but differ in frequency by the oscillator

[5] Hyun-Gwon Kil, Jacek Jarzynski, Yves Berthelot. "Wave decomposition of the vibrations of a cylindrical shell with an automated scanning laser vibrometer", Journal of the Acoustical Society of America, November 1998.

frequency.

D: mirror; reflects the diverging beams coming out of the AOM (C)

E: mirror; reflects only one beam

F: mirror; reflects only one beam, shifted by 40MHz from the beam that is being reflected by mirror E

G-I: beam-fiber coupler; focuses airborne light beam into the core of an optical fiber.

G- used for the reference leg in out of plane detection

H- used as signal leg for out of plane detection or as one of the legs in the in-plane detection

I- used as other leg in the in-plane detection

J: beamsplitter cube; used for re-combination of the reference leg and signal leg in out of plane detection

K: focusing lens; used to focus the recombined interference signal onto the active surface of the optical detector (avalanche photodiode)

L: Avalanche photodiode; used to convert the optical signal beam into an electrical signal for digitization, storage, and analysis

M: optical probe head; used to focus and aim the light beams onto the subject test surface and collect the reflected (specular and diffuse) light from the surface

N: test surface; the object whose motion is to be detected

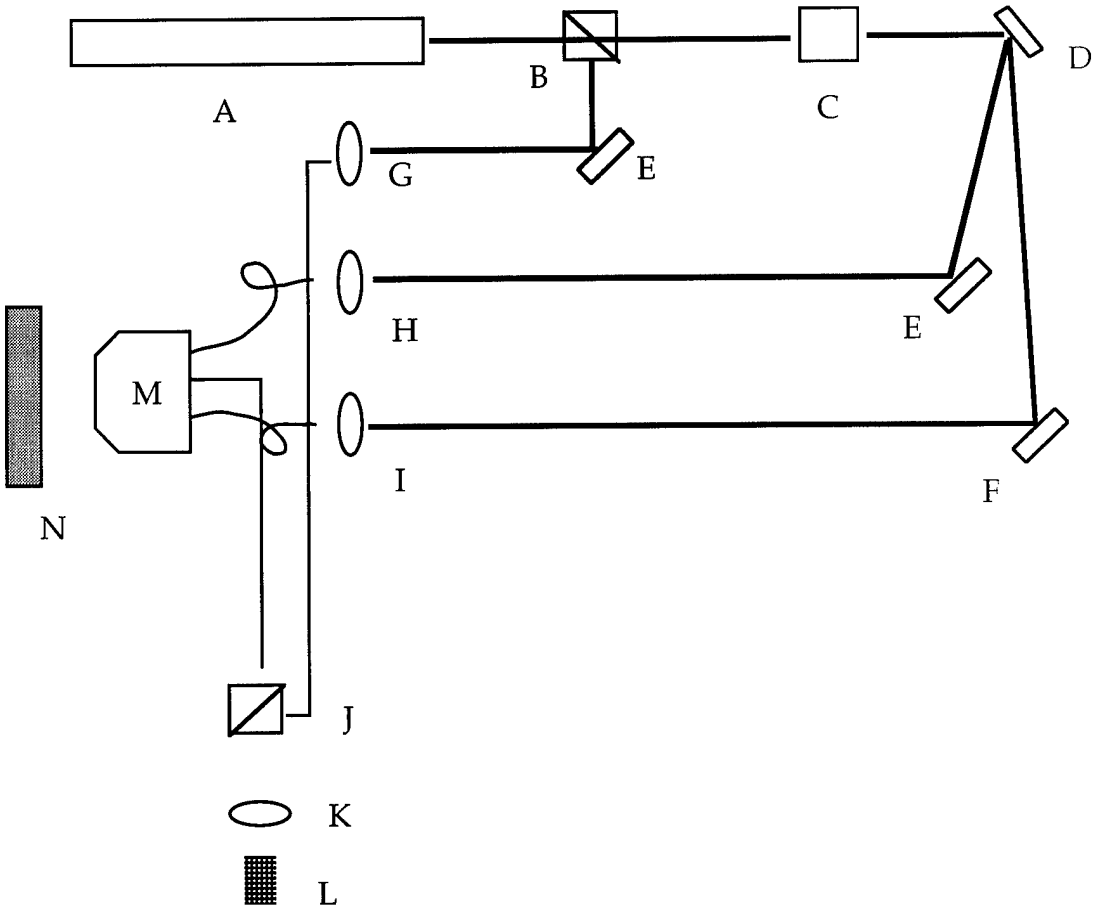

figure 18: LDV setup schematic

The optical probe head utilized GRIN lenses mounted on adjustable springs. The optical fibers were positioned using small diameter tubing and custom-built holders. See figure 19.

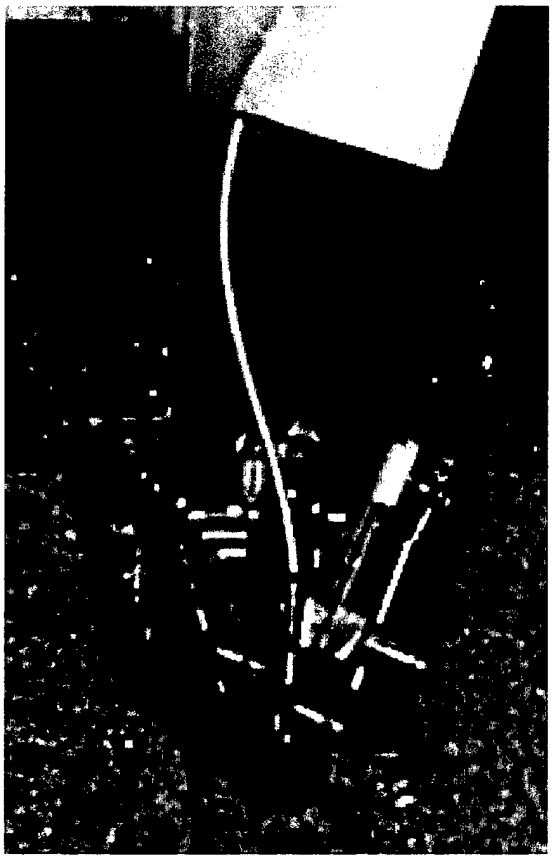

figure 19: close-up view of the optical probe head

For more details on the operation of the LDV system and Laser Doppler Vibrometry, please refer to "Wave decomposition of the vibrations of a cylindrical shell with an automated scanning laser vibrometer" by Hyun-Gwon Kil, Jacek Jarzynski, and Yves Berthelot. Also, The Laser Doppler Technique by L.E. Drain (New York: John Wiley and Sons, 1980) is an excellent source for information on Laser Doppler Vibrometry.

Appendix B
Simplex Computer Code

This code was programmed from the FORTRAN code listed in the Numerical Recipes[6] book, based on the work of Nelder and Mead. A test Simplex solution is presented here for a 2-dimensional function. A plot has been made of the solution simplexes to aid in visualizing the search path of the algorithm.

[6] Numerical Recipes: The Art of Scientific Computing. (New York: Cambridge University Press, 1986).

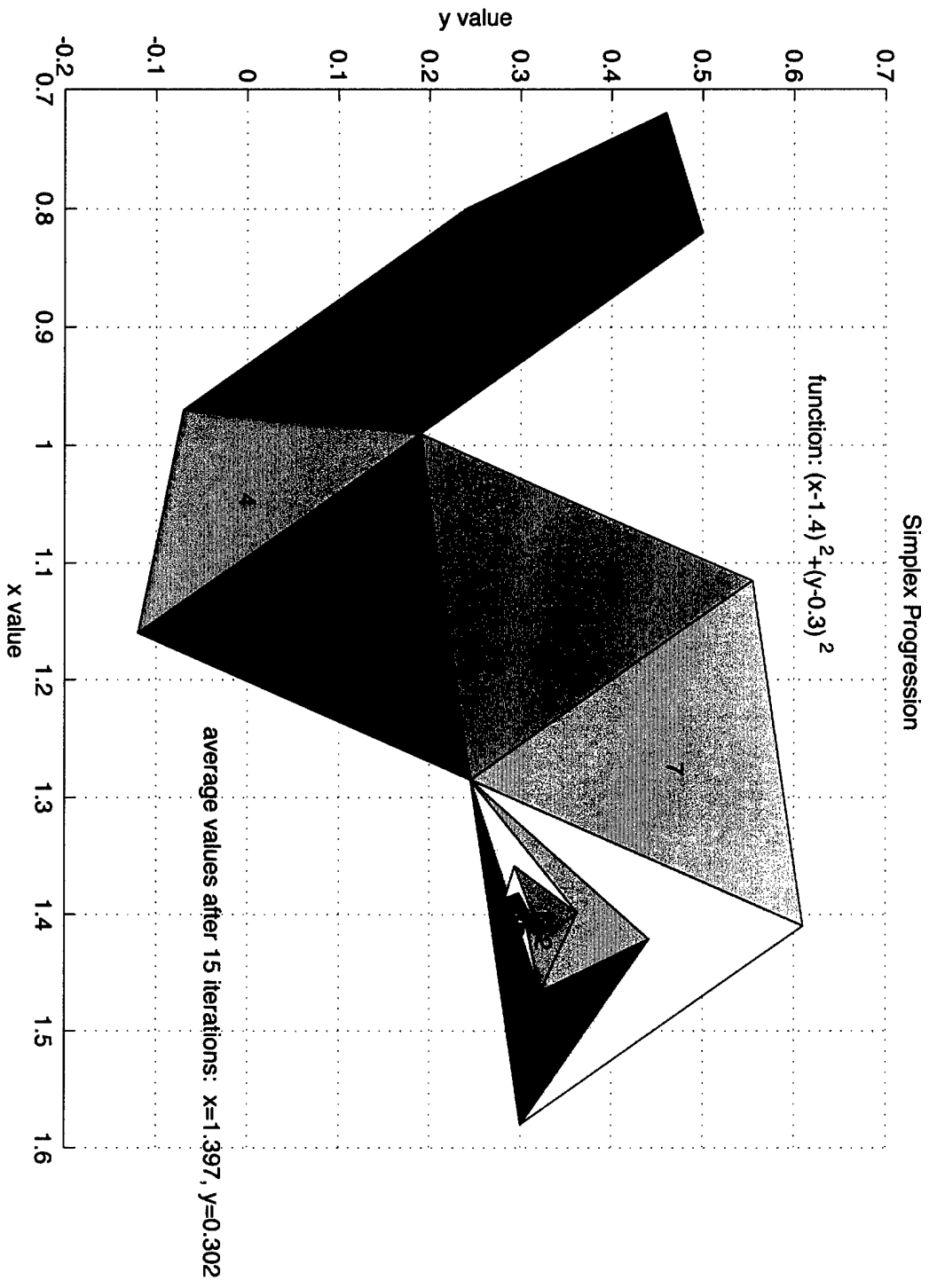

figure 20: sample Simplex result for a simple function

The Simplex solution code was translated from the FORTRAN code in Numerical Recipes and is presented here.

```
function simplex2000(p,ftol,itmax,alpha,beta,gamma)
% From Numerical Recipes page 292-  Nelder and Mead alogrithm
% programmed March 13, 2000
%
% usage: simplex2000(p,ftol,itmax,alpha,beta,gamma)
%       set p=0 for automatic generation
%       omit alpha, beta, gamma for default values

% debugging option- commentary
do_comments=0;

% code for visually tracking progression
newFig=figure('units','norm','position',[0,0,1,1]);
set(gcf,'units','pixels');
figPos=get(gcf,'position');
scrnSize=figPos(3:4);
xlabel('x value');ylabel('y value');
title('Simplex Progression')
grid
%delete(newFig);

% Create an initial simplex if one was not passed in
if p==0,
        p=[0.7,0.2;0.8,0.24;0.72,0.46];
end;

% Set alpha, beta, and gamma if not passed in
if nargin==3,
        alpha=1;
        beta=0.5;
        gamma=2.0;
end;

ndim=size(p,1)-1;
mpts=ndim+1;
```

```
iter=0;
for index=1:size(p,1),
        y(index)=sfn([p(index,1),p(index,2)]);
end;

rtol=2*ftol;
while abs(rtol)>ftol,     % [10]
        ilo=1;
        if y(1)>y(2),
                ihi=1;
                inhi=2;
        else
                ihi=2;
                inhi=1;
        end

        for index=1:mpts,         %[11]
                if y(index)<y(ilo),ilo=index;,end;
                if y(index)>y(ihi),
                        inhi=ihi;
                        ihi=index;
                elseif y(index)>y(inhi),
                        if(index~=ihi),inhi=index;,end;
                end;
        end;                      %[11]

        rtol=2*abs(y(ihi)-y(ilo))/(abs(y(ihi))+abs(y(ilo)));
        if iter==itmax
                disp('exceeding max iterations')
                p
                [sum(p(:,1)/3),sum(p(:,2)/3)]
                pause
        end;

        iter=iter+1;
        for jndex=1:ndim,         % [12]
                pbar(jndex)=0;
        end;                      % [12]
```

```
    for index=1:mpts,       %     [14]
        if index~=ihi,
            for jndex=1:ndim,       %     [13]
                pbar(jndex)=pbar(jndex)+p(index,jndex);
            end;%                                   [13]
        end;
    end;%                               [14]

    if do_comments==1,
        disp('extrapolate by alpha through face')       % -->
    end;

    for jndex=1:ndim,       % [15]
        pbar(jndex)=pbar(jndex)/ndim;
        pr(jndex)=(1+alpha)*pbar(jndex)-alpha*p(ihi,jndex);
    end;%                               [15]

    if do_comments==1,
        disp('evaluate at reflected point')  % -->
    end;

    ypr=sfn(pr);

    if ypr<y(ilo),

        if do_comments==1,
            disp('result better than best, so extrapolate by gamma')
% -->
        end;

        for jndex=1:ndim,       % [16]
            prr(jndex)=gamma*pr(jndex)+(1-gamma)*pbar(jndex);
        end;                    % [16]
        yprr=sfn(prr);
        if yprr<y(ilo),

            if do_comments==1,
                disp('additional extrapolation succeeded, replacing
highest point')    % -->
```

```
                end;

                for jndex=1:ndim,               % [17]
                    p(ihi,jndex)=prr(jndex);
                end;                            % [17]
                y(ihi)=yprr;
            else

                if do_comments==1;
                    disp('additional extrapolatio failed, still using
reflected point')  % -->
                end;

                for jndex=1:ndim,               % [18]
                    p(ihi,jndex)=pr(jndex);
                end;                            % [18]
                y(ihi)=ypr;
            end;
        elseif ypr>y(inhi),

            if do_comments==1,
                disp('reflected point is worse thans second highest')
% -->
            end;

            if ypr<y(ihi),

                if do_comments==1,
                    disp('better than highest, replacing')      % -->
                end;

                for jndex=1:ndim,               % [19]
                    p(ihi,jndex)=pr(jndex);
                end;                            % [19]
                y(ihi)=ypr;
            end
            for jndex=1:ndim,       % [21]
                prr(jndex)=beta*p(ihi,jndex)+(1-beta)*pbar(jndex);
            end;                    % [21]
```

```
            yprr=sfn(prr);
            if yprr<y(ihi),

                  if do_comments==1,
                        disp('contraction was improvement')      % -->
                  end;

                  for jndex=1:ndim,       % [22]
                        p(ihi,jndex)=prr(jndex);
                  end;%                                    [22]
                  y(ihi)=yprr;
            else

                  if do_comments==1,
                        disp('contracting around lowest point')  % -->
                  end;

                  for index=1:mpts,             % [24]
                        if index<ilo,
                              for jndex=1:ndim,       % [23]

pr(jndex)=0.5*(p(index,jndex)+p(ilo,jndex));
                                    p(index,jndex)=pr(jndex);
                              end;                    % [23]
                              y(index)=sfn(pr);
                        end;
                  end;                              % [24]
            end;
      else
            for jndex=1:ndim,             % [25]
                  p(ihi,jndex)=pr(jndex);
            end;                          % [25]
            y(ihi)=ypr;
      end;

      if ndim==2,
            hold on
                  fill(p(:,1),p(:,2),rand(1,3));
                  text((sum(p(:,1)))/3,(sum(p(:,2)))/3,num2str(iter));
```

```
            hold off
        end;

        if ndim==3,
            hold on

            hold off
        end;

end;  % [10]

disp(['final values are: '])
p
[sum(p(:,1)/3),sum(p(:,2)/3)]

disp(' ');disp(['on ', num2str(iter),' iterations'])

function out=sfn(inputArgs)
        if length(inputArgs)==2,
            x=inputArgs(1);y=inputArgs(2);
            out=(x-1.4)^2+(y-0.3)^2;
        elseif length(inputArgs)==3,
            x=inputArgs(1);y=inputArgs(2);z=inputArgs(3);
            out=(x-1.4)^2+(y-0.3)^2+(z+2.7)^3;
        end;
```

Appendix C

Weaver/Hankel Model Code

The Hankel Inverse Transform code derived from Weaver's paper is presented here.

```
% Calculates propagation of elastic waves along the surface.MillerP.m
% with z=0. Calculates the generation of elastic waves by a normal
% load on the surface of a layer on rigid back. Based on the
% integral transform solution of Weaver.
% Includes integration using Simpson 1/3 rule.
% Calculation of propagation of the transient signal
% Uses accelerometer signal as the drive - pulse(n)

 clear all;

load drive2p.dat;

% program to create a one cycle sine wave pulse,
% which is the drive signal.

for n=1:256
pulse(n)=0;
end

dtau=2.4e-5;

for n=1:256
pulse(n)=drive2p(n);
end

%create time array

for n=1:256
time(n)=(n-1)*dtau;
end

%Fourier transform of the drive pulse
```

```
Fc=fft(pulse);

% create propagator array for given
% position of observation point and drive point
a=0.0025;
r=0.064;
% z=0.0;

% properties of layer material
L=0.05;

% frequency loop

delfr=1/(dtau*256);

for l=1:128
uzarr(l)=0;
end

for l=2:128
sho=l
frarr(l)=(l-1)*delfr;
freq=frarr(l);
clr=2.418e+1*log(freq) + 7.303e+1;
cli=8.621*log(freq) - 2.152e+1;
csr=9.535*log(freq) + 2.857e+1;
csi=3.332*log(freq) - 8.019;
cl=clr+i*cli;
cs=csr+i*csi;

omeg=2*pi*freq;
k1=omeg/cl;
k2=omeg/cs;
rk2=real(k2);
k2p=k2/rk2;
k1p=k1/rk2;
delk2p=1/500;
ap=a*rk2;
rp=r*rk2;
```

```
Lp=L*rk2;

% integrand array for uz

clear zetapt v1pt besst uzintt

zmax=round(61-0.3*l);
zetapt=0:delk2p:zmax;
max=zmax/delk2p+1;
uzintt=zeros(1,max);
v1pt=sqrt(k1p*k1p-zetapt.*zetapt);
besst=bessel(1,ap*zetapt).*bessel(0,rp*zetapt);

%check maximum value of v1pt

if -imag(v1pt(max))*Lp<150
 ind=1;
else
 ind=2;
end

if ind==2
 mdiv=round(150/(Lp*delk2p));
end

% develop full or asymptotic expression for the
% z and r integrands.If ind=1 use full expression
% for uz and ur over the entire range of zetapt.
% If ind=2 use full expression for zetap less than
% or equal to mdiv and the asymptotic expression
% for zetap greater than mdiv.

if ind==1
fzetat=(2*(zetapt.*zetapt)-k2p*k2p);
v1t=sqrt(zetapt.*zetapt-k1p*k1p);
v2t=sqrt(zetapt.*zetapt-k2p*k2p);
v2pt=sqrt(k2p*k2p-zetapt.*zetapt);
c1pt=2*v1t./fzetat;
c3pt=c1pt.*((zetapt.*zetapt).*cos(Lp*v2pt))-v1t.*cos(Lp*v1pt);
```

```
d1pt=(c1pt.*(zetapt.*zetapt).*(cos(Lp*v1pt).*cos(Lp*v2pt)));
d1pt=d1pt+(c1pt.*(v1t.*v2t)).*(sin(Lp*v1pt).*sin(Lp*v2pt))-v1t;
d2pt=(c1pt.*v2t).*(zetapt.*zetapt)-(v1t.*v2t).*(cos(Lp*v2pt).*cos(Lp*v1pt));
d2pt=d2pt-(zetapt.*zetapt).*(sin(Lp*v2pt).*sin(Lp*v1pt));

uznumt=((zetapt.*zetapt).*(d1pt.*sin(Lp*v2pt))-v1t.*(d2pt.*sin(Lp*v1pt)))
...
   .*(i*((zetapt.*zetapt).*c1pt-v1t));
uzdent=c3pt.*(fzetat.*d2pt-2*(zetapt.*zetapt).*(v2t.*d1pt));

% integrand arrays for uz and ur

uzintt=(uznumt./uzdent).*besst;
clear fzetat
clear v1t v2t v2pt c1pt c3pt d1pt
clear d2pt uznumt uzdent
end

if ind==2

zetap=zetapt(1:mdiv);
zetapa=zetapt(mdiv+1:max);

bess=besst(1:mdiv);
bessa=besst(mdiv+1:max);

fzeta=(2*(zetap.*zetap)-k2p*k2p);
v1=sqrt(zetap.*zetap-k1p*k1p);
v2=sqrt(zetap.*zetap-k2p*k2p);
v1p=sqrt(k1p*k1p-zetap.*zetap);
v2p=sqrt(k2p*k2p-zetap.*zetap);
c1p=2*v1./fzeta;
c3p=c1p.*((zetap.*zetap).*cos(Lp*v2p))-v1.*cos(Lp*v1p);
d1p=(c1p.*(zetap.*zetap).*(cos(Lp*v1p).*cos(Lp*v2p)));
d1p=d1p+(c1p.*(v1.*v2)).*(sin(Lp*v1p).*sin(Lp*v2p))-v1;
d2p=(c1p.*v2).*(zetap.*zetap)-(v1.*v2).*(cos(Lp*v2p).*cos(Lp*v1p));
d2p=d2p-(zetap.*zetap).*(sin(Lp*v2p).*sin(Lp*v1p));

uznum=i*((zetap.*zetap).*(d1p.*sin(Lp*v2p))-v1.*(d2p.*sin(Lp*v1p))) ...
```

```
    .*((zetap.*zetap).*c1p-v1);
uzden=c3p.*(fzeta.*d2p-2*(zetap.*zetap).*(v2.*d1p));

% integrand arrays for uz in the full region

uzintt1=(uznum./uzden).*bess;
uzintt(1:mdiv)=uzintt1;

clear zetap fzeta bess
clear v1 v2 v1p v2p c1p c3p d1p
clear d2p uznum uzden uzintt1

fzetaa=(2*(zetapa.*zetapa)-k2p*k2p);
v1a=sqrt(zetapa.*zetapa-k1p*k1p);
v2a=sqrt(zetapa.*zetapa-k2p*k2p);
v1pa=sqrt(k1p*k1p-zetapa.*zetapa);
v2pa=sqrt(k2p*k2p-zetapa.*zetapa);
c1pa=2*v1a./fzetaa;
uznuma=((zetapa.*zetapa).*c1pa-v1a).*((zetapa.*zetapa).*c1pa ...
   .*exp((abs(v1pa)-abs(v2pa))*Lp) - v1a);
uzdena=((zetapa.*zetapa).*c1pa.*exp((abs(v1pa)-abs(v2pa))*Lp)-v1a) ...
    .*(fzetaa-2*v2a.*(zetapa.*zetapa).*c1pa);
uzintta=(uznuma./uzdena).*bessa;

uzintt(mdiv+1:max)=uzintta;

clear zetapa fzetaa bessa bessra
clear v1a v2a v1pa v2pa c1pa c3pa d1pa
clear d2pa uznuma uzdena uzintta

end

% integrate the arrays uzintt

n=zmax*500;
uzfr=uzintt(1)+4*sum(uzintt(2:2:n))+uzintt(n+1);
uzfr=uzfr+2*sum(uzintt(3:2:n));
uzfr=(delk2p/3)*uzfr;
```

```
uzarr(l)=uzfr;
vzarr(l)=i*omeg*uzarr(l);

end

frarr(1)=0;
uzarr(1)=uzarr(2);
vzarr(1)=vzarr(2);

% create inverse Fourier transform of ur,uz and vr,vz signals

for n=1:128
uzinvs(n)=uzarr(n)*Fc(n);
vzinvs(n)=vzarr(n)*Fc(n);
end

for n=130:256
k=n-130;
uzinvs(n)=conj(uzinvs(128-k));
vzinvs(n)=conj(vzinvs(128-k));
end

uzinvs(129)=uzinvs(1);
vzinvs(129)=vzinvs(1);

%Take inverse Fourier transform to generate uz and vz,
%and ur and vr signals at r,z=0

siguz=ifft(uzinvs);
sigvz=ifft(vzinvs);

%plot(time,.01*pulse,'b')
%hold
%plot(time,real(siguz),'r')
plot(time(1:100),real(-sigvz(1:100)),'r')

end
```

Appendix D

Finite Element Modelling

In section VII, Comments and Conclusions, some discussion and results were presented for work done on cavity detection capability with the current system. In addition to this experimental work there was some finite element modelling to investigate the effects and detectability of an occlusion in a sample of the type analyzed in the present work.[7] The modelling was intended to analyze the influence of a cavity on the motion at the interface between the polymer material and medium, in the case air (free surface of sample).

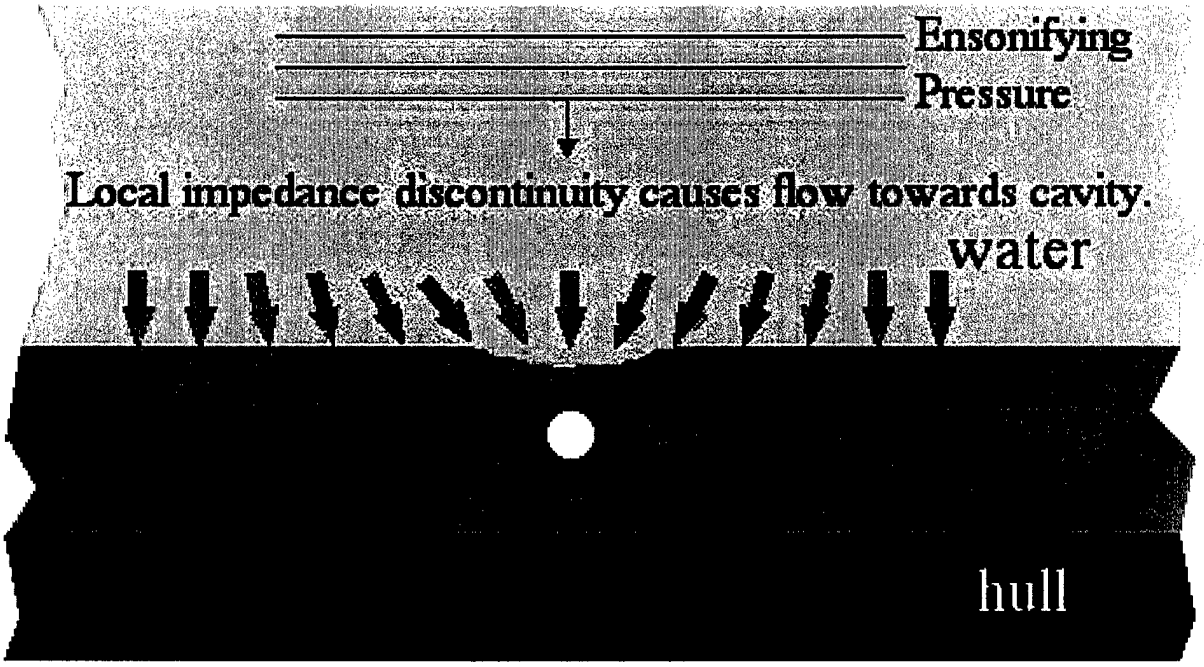

figure 21: local impedance discontinuity causes flow towards cavity

[7] Caspall, Jayme. "Dynamics of Cavities in Layered Media." Presentation given as part of the In-Situ Coating Program review presented on 19 August 1997.

Figure 21 depicts the way that mass in the sample will tend to flow towards the cavity in the layer. Since there is a mass flow induced by the impedance discontinuity there will be an associated resonance from the effective spring caused by the impedance and mass flow. A resonance of this type is of interest in the case where sensors are attached to the free surface of the sample layer. When positioned as a linear array, the sensors' output will be affected by the noise generated from the nonuniform surface motion.

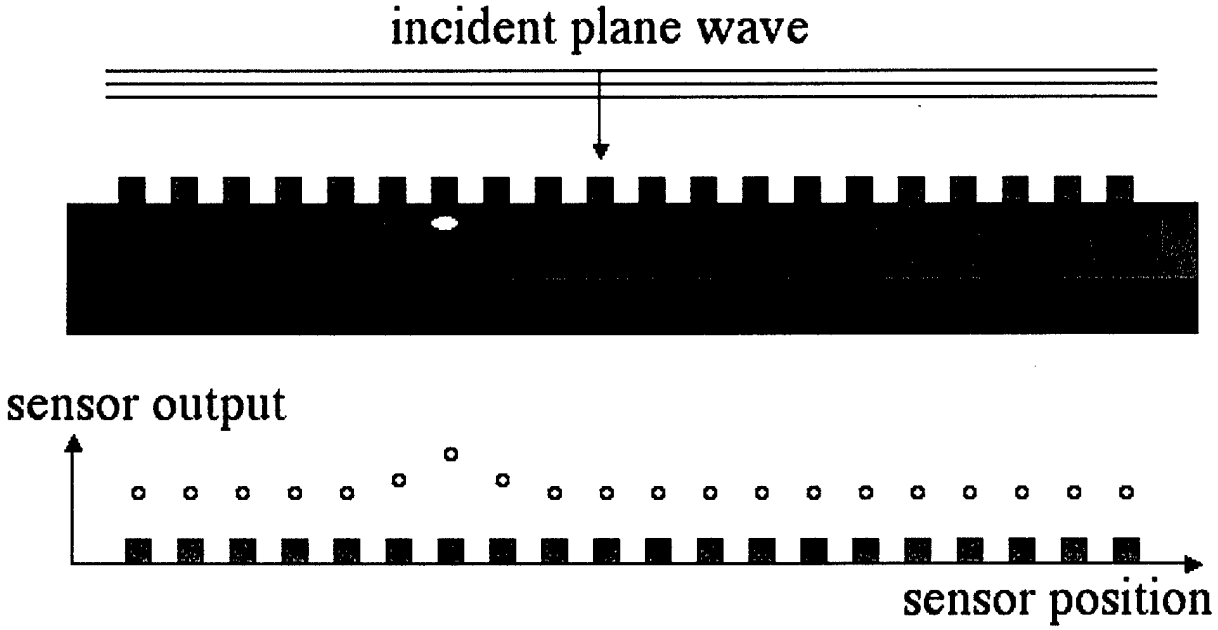

figure 22: nonuniform sensor output

Finite element models were created using Sara 2D[8] . One of them was used to investigate the effect of cavity depth on resonance and the other the effect of cavity height on resonance. In the former, a cavity is

[8] "Sara 2D" by BBN Systems and Technologies, Union Station, New London, CT 06320-6147.

inserted at the free surface and its size in the axial direction varied. In the latter the cavity is inserted at the constrained surface (polymer lab bonded to steel plate) and grows axially.

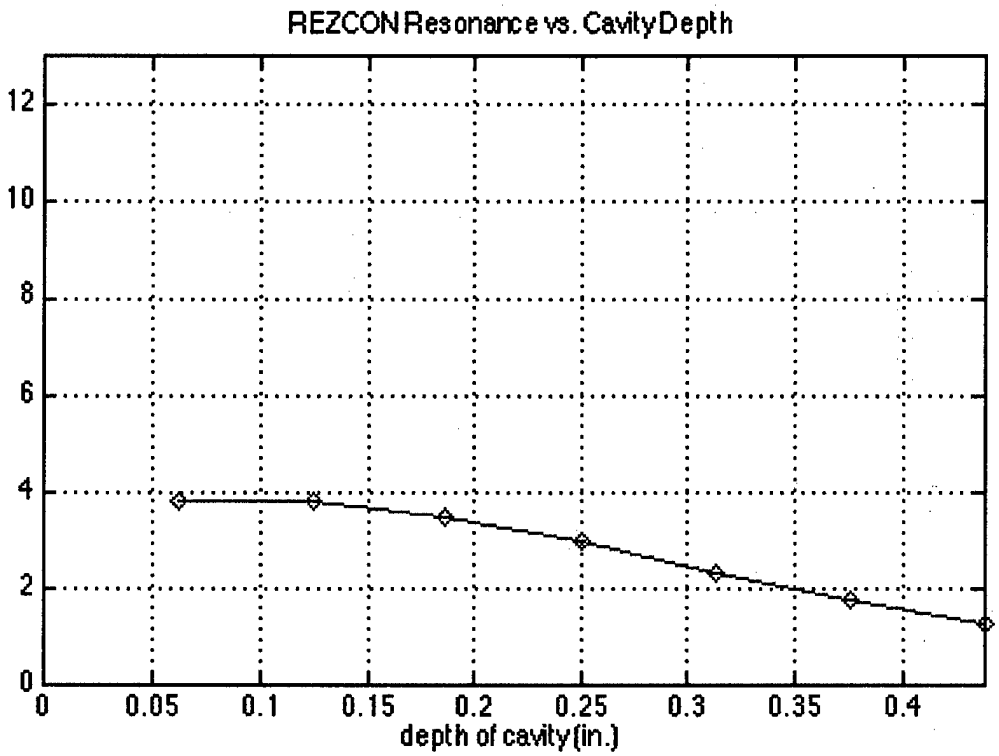

figure 23: effect of cavity depth on resonance; vertical axis shows reduction in resonance frequency compared to no cavity, %

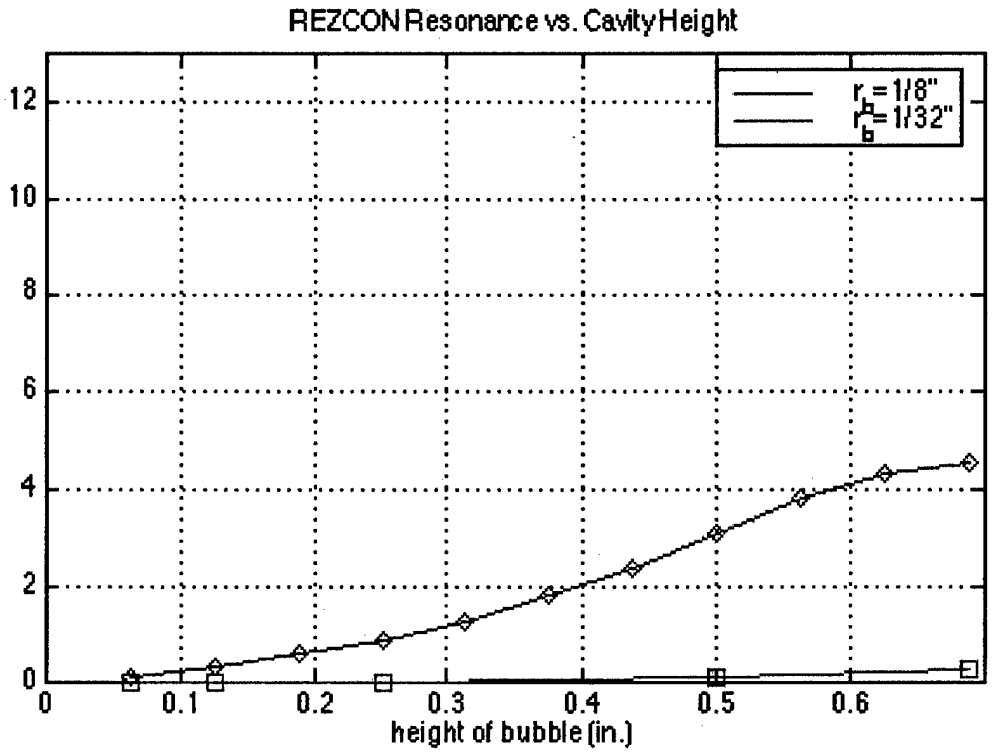

figure 24: effect of cavity height on resonance; vertical axis shows reduction in resonance frequency compared to no cavity, %

A third FEM was used to see the effect of cavity radius on resonance.

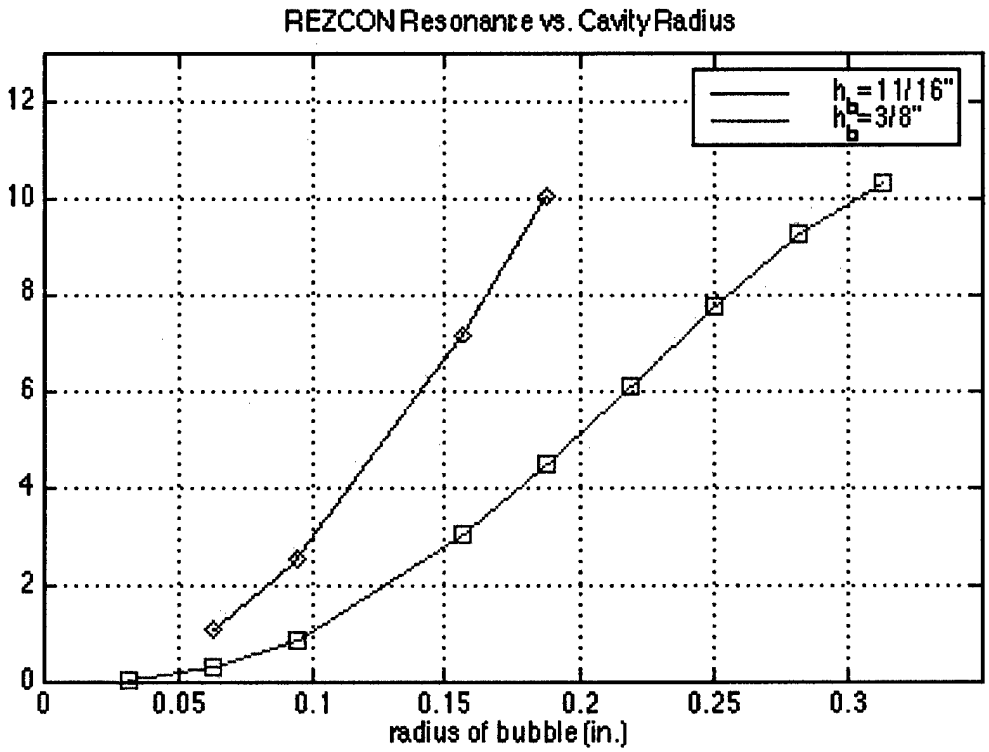

figure 25: effect of cavity radius on resonance; vertical axis shows reduction in resonance frequency compared to no cavity, %

The finite element modelling was used for detectability estimation using a two-dimensional plane strain model. The load was a unit line force and the cavity was treated as an infinite cylindrical free boundary within the coating. The velocity was calculated for various distances from the line force and covered a range commensurate with actual measurements. Plots are shown comparing the "with-cavity" case to the "without-cavity" case and the calculations are repeated for various cavity diameters and various cavity depths.

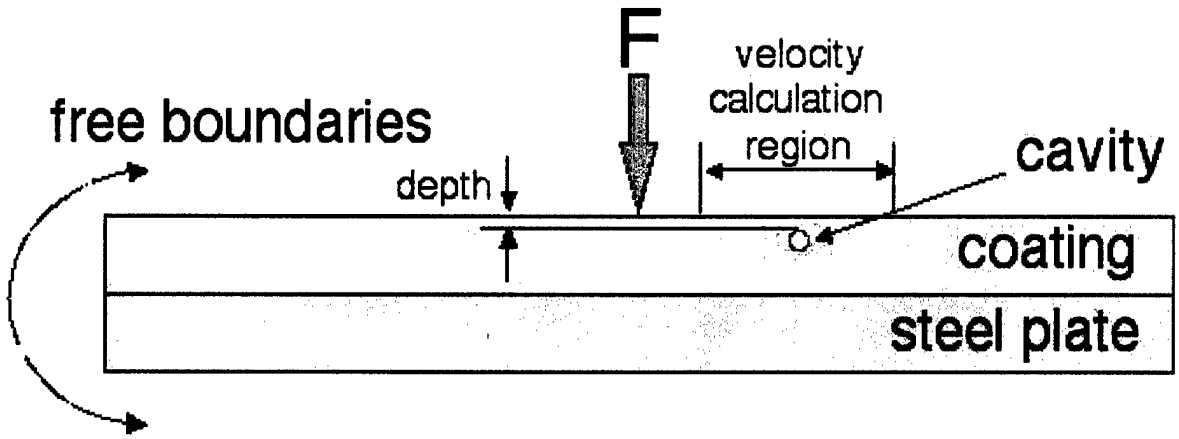

figure 26: FEM used for detectability estimation

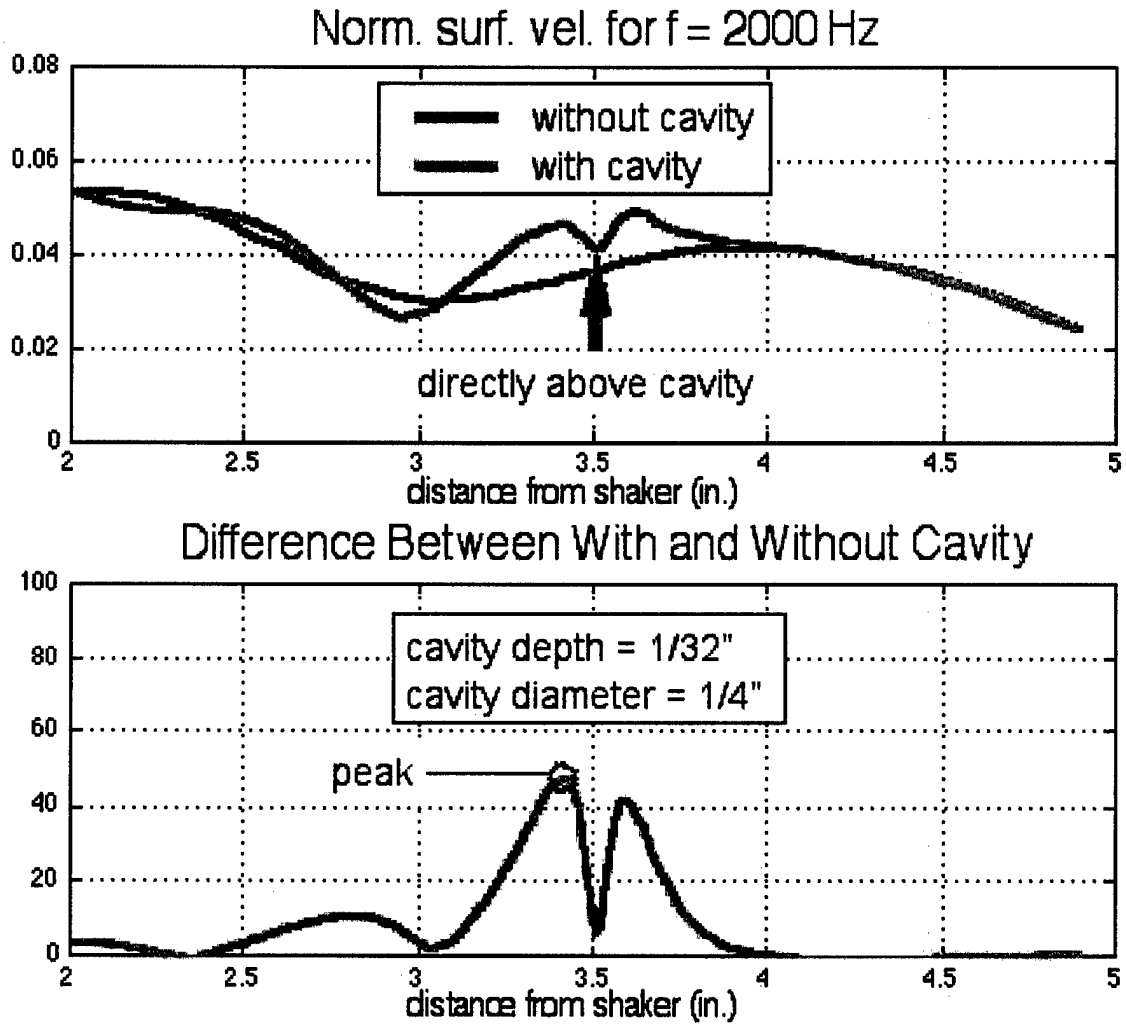

figure 27: use of FEM results

The model results are shown in figure 27. At a given frequency, the peak relative difference in the amplitude of the normal surface velocity between the with-cavity and the without-cavity case is calculated for each cavity diameter and depth. The calculated difference is compared to he experimentally determined minimum detectable difference.

Figure 28,29, and 30 are cavity detectability matrices from model calculations. Each shows the detectability status for combinations of frequency, cavity diameter, and cavity depth. Figure 28 shows results based on current capabilities, figure 29 shows results with an attainably better system, and figure 30 shows a cumulative report.

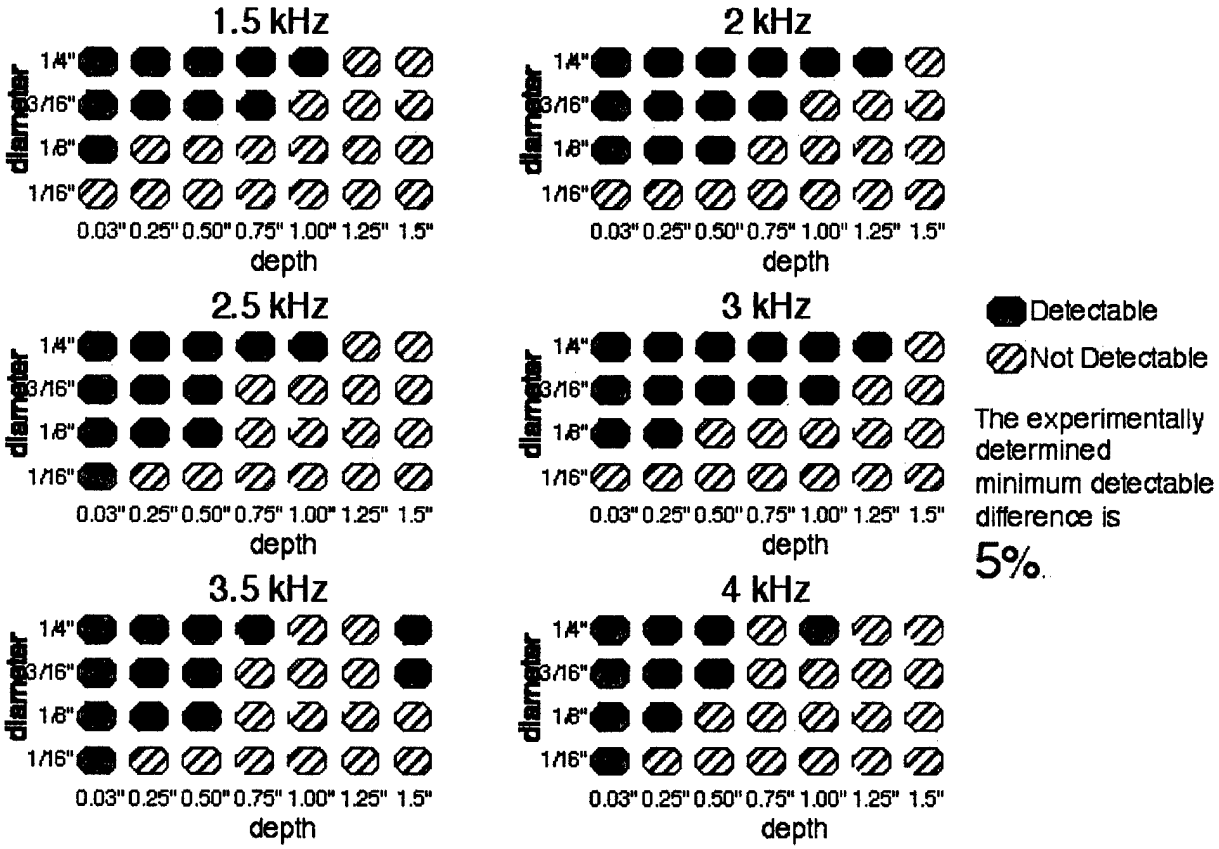

figure 28: cavity detectability matrix for current system

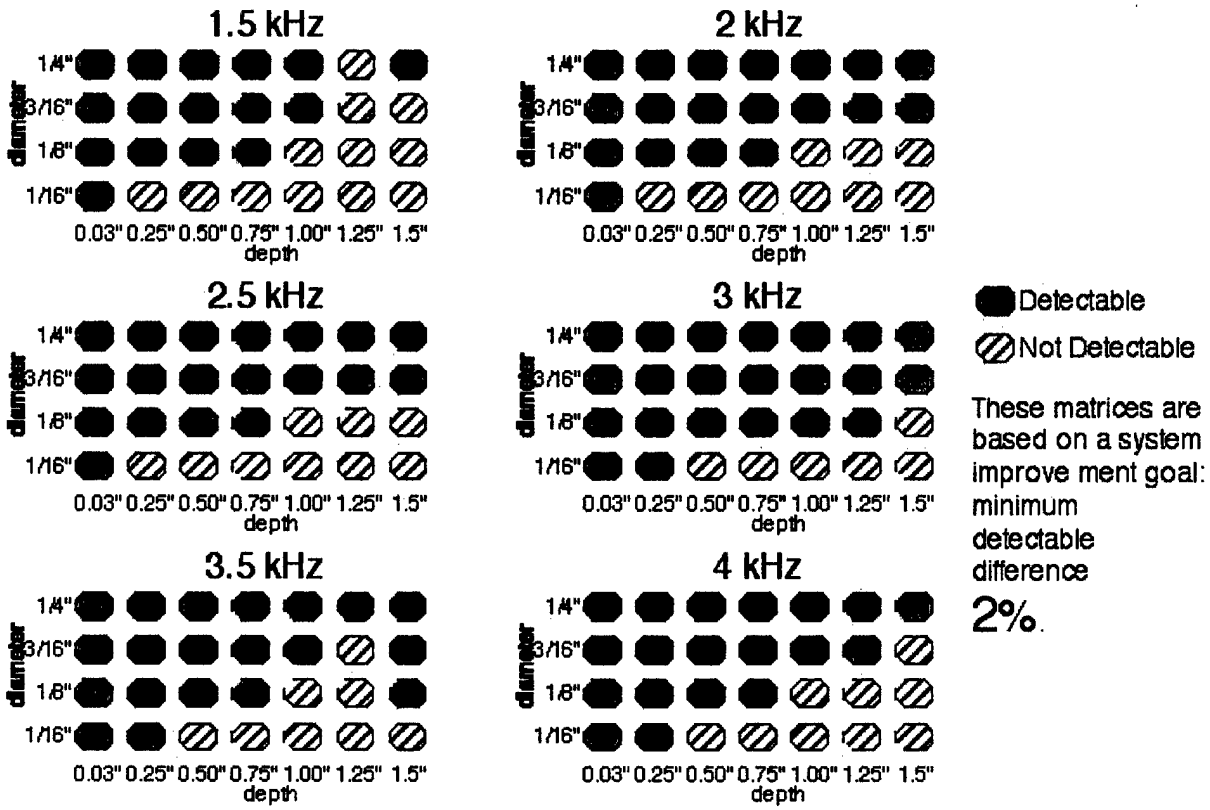

figure 29: cavity detection based on improved system

Cumulative Detectabilities (1.5 kHz - 4 kHz)*

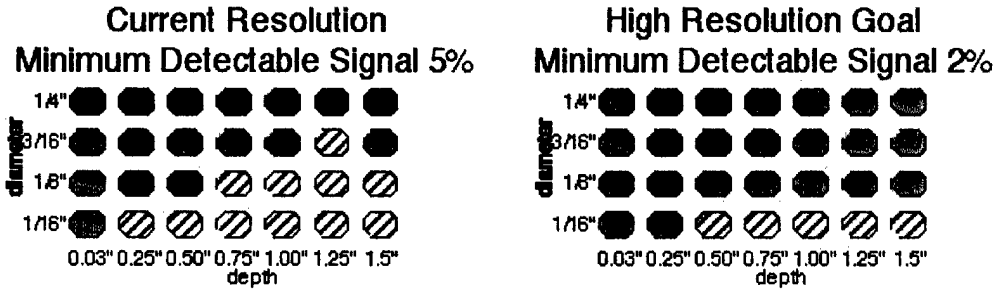

*Note: 4 kHz is the highest frequency allowed by the model. The fundamental cavity resonance is higher than 4 kHz. The 1/4" cavity has the lowest resonance frequency of all the cavities in the study at approximately 7 kHz. Scattering results for the case of a spherical cavity in an infinite homogeneous medium suggests that the resonance provides the largest signals for detection.

figure 30: cumulative detectability

Some analytical calculations were done to look at the effects of detecting scattered signals from an occlusion at resonance versus not at resonance. The scattering calculations are based on the formulation of Graff with plane wave incidence.[9] In reference to the plots, the cavity is centered at x=0 and the detection threshold is provided as a reference only. The scattering formulation assumes an infinite medium and cannot provide accurate detection estimates for the case of a coating layer on a steel plate.

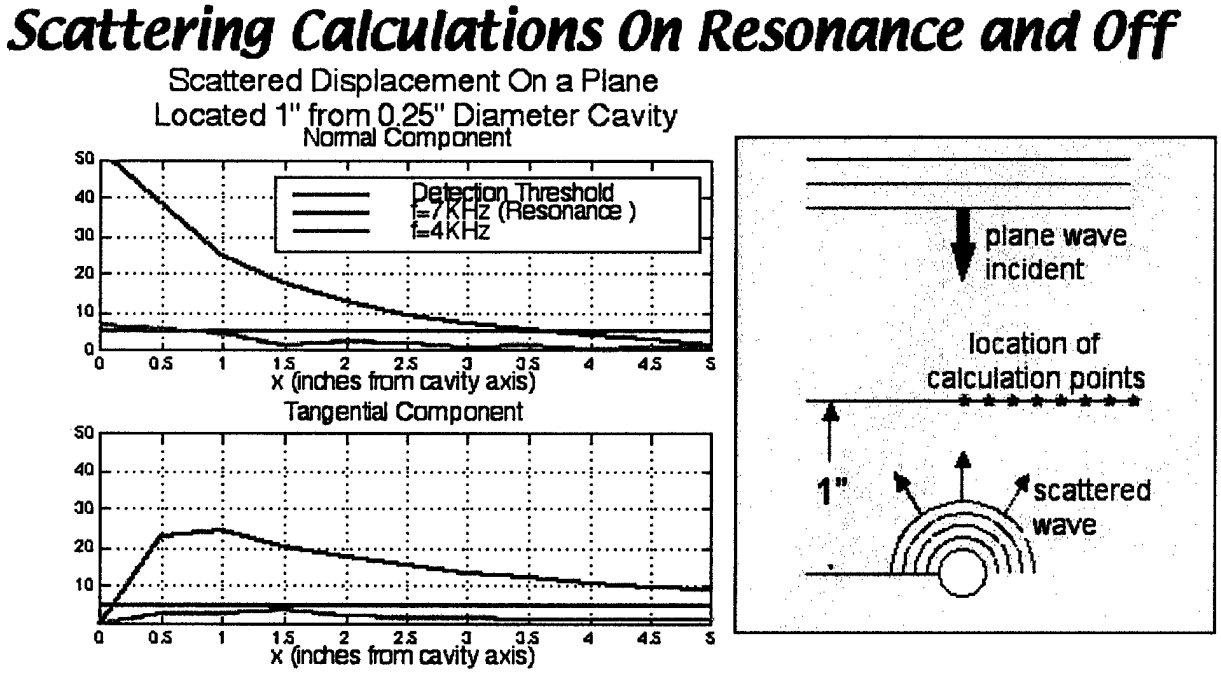

figure 31: scattering calculations on resonance and off

[9] Graff, Karl F. Wave Motion in Elastic Solids. (New York: Dover Publications,1973).

REPORT DOCUMENTATION PAGE

Form Approved
OMB No. 0704-0188

1. AGENCY USE ONLY (Leave Blank)	2. REPORT DATE	3. REPORT TYPE AND DATES COVERED
	31 March 2000	Final Technical Report 15 Oct 1995 - 31 Mar 2000

4. TITLE AND SUBTITLE
Proposal for In-Situ Determination of Acoustic Parameters of Navy Coatings for Mold-in-Place Application

5. FUNDING NUMBERS
N00014-96-1-0175

6. AUTHOR(S)
John Doane

7. PERFORMING ORGANIZATION NAME (S) AND ADDRESS(ES)
Georgia Tech Research Institute
Georgia Institute of Technology
Undersea Research Program Office
Atlanta, Georgia 30332

8. PERFORMING ORGANIZATION REPORT NUMBER
A-5133

9. SPONSORING/MONITORING AGENCY NAME(S) AND ADDRESS(ES)
Office of Naval Research
Richard Vogelsong, Code 334
Ballston Centre Tower One
800 North Quincy Street
Arlington, VA 22217-5660

10. SPONSORING/MONITORING AGENCY REPORT NUMBER

11. SUPPLEMENTARY NOTES

12a. DISTRIBUTION/AVAILABILITY STATEMENT
APPROVED FOR PUBLIC RELEASE

12b. DISTRIBUTION CODE

13. ABSTRACT (Maximum 200 words)

This report documents the research completed on grant N00014-96-0175, In-Situ Determination of Acoustic Parameters of Navy Coatings for Mold In-Place Application, also known as LDV Measurements of Hull Treatment Properties.

The objective of this project was to develop a method for in-situ determination of acoustic quality and performance of the mold in-place coatings. The physical parameters which determine the acoustical performance are the complex longitudinal and shear moduli. These properties were determined in-situ by driving the coating with a broadband transient impulse and measuring the surface motion at several points using a laser Doppler probe.

In March 2000 the research effort concluded with a set of data points for the test material of interest. This data represents the culmination and integration of several aspects of the work including the recording of ten LDV waveforms, development of an Acoustical Ray Model, half-space definite-integral model, and a complete Hankel-transform model. The data and the models were processed by a Simplex optimization routine to output the desired quantities.

The project's achieved level of success shows that this technique could provide a solution to the in-situ properties determination problem with refinement of some aspects of the technique.

14. SUBJECT TERMS
coating materials
laser Doppler velocimetry

15. NUMBER OF PAGES
70

16. PRICE CODE

17. SECURITY CLASSIFICATION OF REPORT	18. SECURITY CLASSIFICATION OF PAGE	19. SECURITY CLASSIFICATION OF ABSTRACT	20. LIMITATION OF ABSTRACT
UNCLASSIFIED	UNCLASSIFIED	UNCLASSIFIED	SAR

NSN 7540-01-280-5500

Standard Form 298 (Rev. 2-89)
Prescribed by ANSI Std. Z39-18
298-102